Hydrothermal and tectonic activity in northern Yellowstone Lake, Wyoming

Samuel Y. Johnson[†]
William J. Stephenson[‡]
Lisa A. Morgan[§]
W.C. Shanks III[#]
U.S. Geological Survey, MS 966, Box 25046, Denver Federal Center, Denver, Colorado 80225, USA
Kenneth L. Pierce[††]
U.S. Geological Survey, P.O. Box 173492, Montana State University, Bozeman, Montana 59717, USA

ABSTRACT

Yellowstone National Park is the site of one of the world's largest calderas. The abundance of geothermal and tectonic activity in and around the caldera, including historic uplift and subsidence, makes it necessary to understand active geologic processes and their associated hazards. To that end, we here use an extensive grid of high-resolution seismic reflection profiles (~450 km) to document hydrothermal and tectonic features and deposits in northern Yellowstone Lake.

Sublacustrine geothermal features in northern Yellowstone Lake include two of the largest known hydrothermal explosion craters, Mary Bay and Elliott's. Mary Bay explosion breccia is distributed uniformly around the crater, whereas Elliott's crater breccia has an asymmetric distribution and forms a distinctive, ~2-km-long, hummocky lobe on the lake floor. Hydrothermal vents and low-relief domes are abundant on the lake floor; their greatest abundance is in and near explosion craters and along linear fissures. Domed areas on the lake floor that are relatively unbreached (by vents) are considered the most likely sites of future large hydrothermal explosions. Four submerged shoreline terraces along the margins of northern Yellowstone Lake add to the Holocene record of postglacial lake-level fluctuations attributed to "heavy breathing" of the Yellowstone magma reservoir and associated geothermal system.

The Lake Hotel fault cuts through northwestern Yellowstone Lake and represents part of a 25-km-long distributed extensional deformation zone. Three postglacial ruptures indicate a slip rate of ~0.27 to 0.34 mm/yr. The largest (3.0 m slip) and most recent event occurred in the past ~2100 yr. Although high heat flow in the crust limits the rupture area of this fault zone, future earthquakes of magnitude ~5.3 to 6.5 are possible. Earthquakes and hydrothermal explosions have probably triggered landslides, common features around the lake margins.

Few high-resolution seismic reflection surveys have been conducted in lakes in active volcanic areas. Our data reveal active geothermal features with unprecedented resolution and provide important analogues for recognition of comparable features and potential hazards in other subaqueous geothermal environments.

Keywords: Yellowstone Lake, seismic reflection profiles, hydrothermal processes, explosive eruptions, extension faults, earthquake hazards.

INTRODUCTION

Yellowstone National Park (Fig. 1) is famous for its geothermal phenomena and other natural wonders. It occupies part of an active volcanic province on the east flank of the Basin and Range and includes one of the world's largest calderas (Christiansen, 2001). Active uplift and subsidence of the caldera floor (Pelton and Smith, 1982; Dzurisin and Yamashita, 1987; Dzurisin et al., 1990, 1994; Wicks et al., 1998) and abundant seismicity (Smith and Arabasz, 1991) confirm the dynamic geologic setting of Yellowstone. To better understand the recent geologic history, processes, and hazards of Yellowstone, we collected high-resolution seismic reflection data (Figs. 2, 3) across northern Yellowstone Lake. Specific questions we address involve the location, quantity, size, geometry, and relative age of hydrothermal features and deposits, the postglacial behavior of the Yellowstone caldera, and the location and histories of active faults.

Here, we report the results of our seismic reflection survey. Seismic profiles show a range of hydrothermal phenomena including explosion craters, explosion-breccia deposits, vents, and low-relief domes. Identification of submerged shoreline terraces adds to the record of lake-level change, an important indicator of the Holocene behavior of the Yellowstone magmatic/geothermal system. High-resolution images of active faults provide paleoseismological data essential for earthquake-hazard assessment.

QUATERNARY GEOLOGY

The Yellowstone Lake basin straddles the southeastern margin of the Yellowstone caldera (Fig. 1). This caldera formed at ca. 640 ka in the last of three major caldera-forming eruptions in the 2.1 to 0 Ma Yellowstone Plateau volcanic field (U.S. Geological Survey, 1972; Christiansen, 1984, 2001). Younger (ca. 150 to 70 ka) rhyolitic volcanic flows subsequently filled in much of the caldera, including parts of the Yellowstone Lake basin. These

[†]E-mail: sjohnson@usgs.gov.
[‡]E-mail: wstephens@usgs.gov.
[§]E-mail: lmorgan@usgs.gov.
[#]E-mail: pshanks@usgs.gov.
[††]E-mail: kpierce@usgs.gov.

GSA Bulletin; August 2003; v. 115; no. 8; p. 954–971; 23 figures; 1 table.

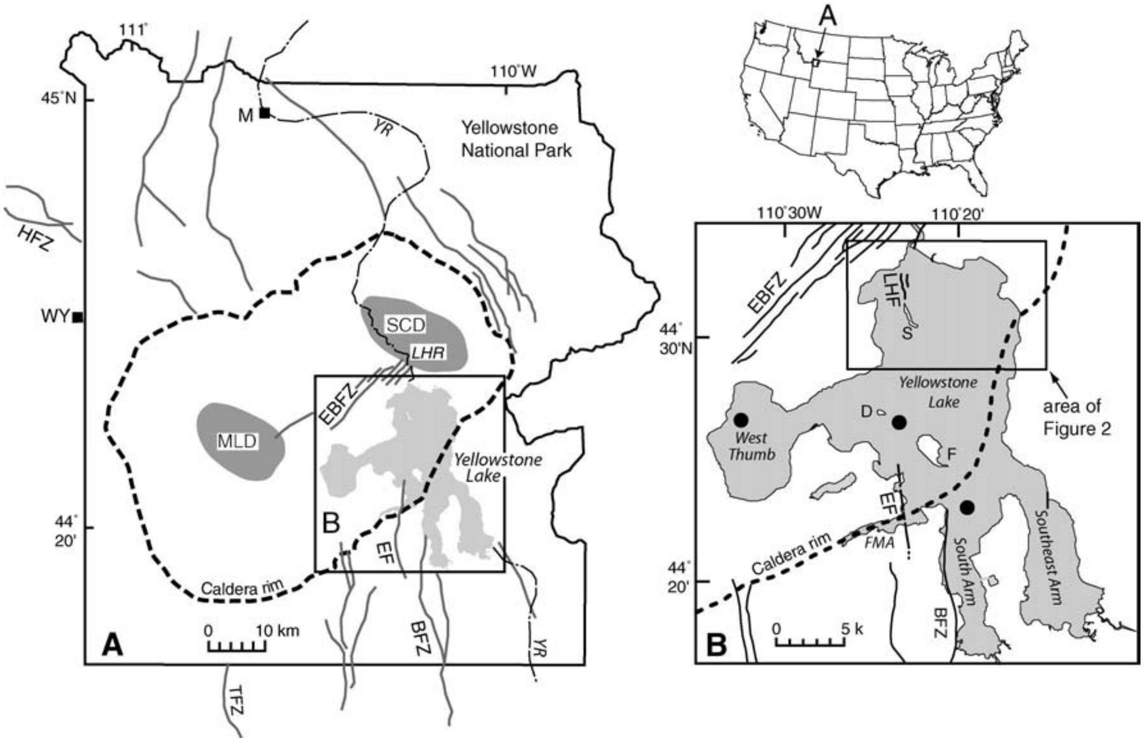

Figure 1. Maps showing location of Yellowstone National Park and Yellowstone Lake, area of Figure 2, and caldera rim (based on Locke and Meyer, 1994; Christiansen, 2001; Finn and Morgan, 2002). BFZ—Buffalo Fork fault zone; D—Dot Island; EBFZ—Elephant Back fault zone; EF—Eagle Bay fault (Richmond, 1974; Locke et al., 1992); F—Frank Island; FMA—Flat Mountain Arm; HFZ—Hebgen fault zone; LHF—Lake Hotel fault; LHR—Le Hardy Rapids; M—Mammoth; MLD—Mallard Lake Dome; S—Stevenson Island; SCD—Sour Creek dome; TFZ—Teton fault zone; WY—West Yellowstone; YR—Yellowstone River. Dots at the north end of the South Arm, between Frank and Dot Islands, and in West Thumb show locations of lake-sediment cores and targeted seismic reflection profiles of Tiller (1995).

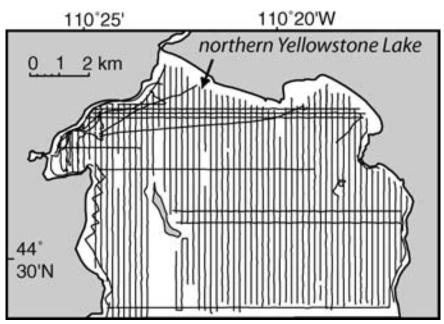

Figure 2. Map showing track lines for seismic reflection survey in northern Yellowstone Lake.

younger flows and caldera resurgence dammed drainages and impounded lakes in the present-day Yellowstone Lake basin (Richmond, 1977a, 1977b). Geodetic investigations document high vertical deformation rates within the caldera and the lake basin that are linked to ongoing underlying magmatic activity (Pelton and Smith, 1982; Dzurisin and Yamashita, 1987; Dzurisin et al., 1990, 1994; Wicks et al., 1998).

The Yellowstone Lake basin was occupied by glaciers several times in the Pleistocene; the last pulse of the most recent Pinedale glaciation retreated at ca. 16 ka (Pierce, 1979; Licciardi et al., 2001; Pierce et al., 2002). Exposed shoreline terraces indicate that shortly after glacial retreat, lake level was ~30 to 35 m higher than at present (Richmond, 1977b; Locke and Meyer, 1994). A suite of younger terraces at lower elevations documents Holocene lake-level fluctuations and overall decline. Development of the terraces is associated with uplift and subsidence of the lake outlet caused by intracaldera processes, such as magma intrusion and cooling, and geothermal inflation and deflation (Locke and Meyer, 1994; Pierce et al., 1997, 2002). On-land shoreline terraces have been variably tilted so that they are not at uniform elevations and thus have utility as markers for evaluating Holocene deformation (Meyer and Locke, 1986; Locke and Meyer, 1994; Pierce et al., 2002).

Muffler et al. (1971) described postglacial hydrothermal-explosion craters adjacent to northern Yellowstone Lake at Indian Pond and Turbid Lake (Fig. 2), and Wold et al. (1977) documented the presence of a submerged hydrothermal crater at Mary Bay within northeastern Yellowstone Lake. Additional geothermal features, including hot springs and geysers, are found in several locations within the Yellowstone Lake basin, most notably at West Thumb (Fig. 1; Remsen et al., 1990; Christiansen, 2001; Morgan et al., 2003).

YELLOWSTONE LAKE

Yellowstone Lake (Fig. 1) is the largest high-elevation (2357 m) lake in North America. It occupies ~340 km² and has a maximum depth of 133 m (Kaplinski, 1991). Large-scale relief on the lake floor and lake margins is controlled by the submerged flanks of postcaldera rhyolitic flows (Morgan et al., 2003) and relict glacial landforms (Otis et al., 1977).

The Yellowstone River is the largest inflow and outflow of water and sediment into Yellowstone Lake (Benson, 1961). The river enters the lake in the Southeast Arm and exits at the lake outlet along the lake's northern

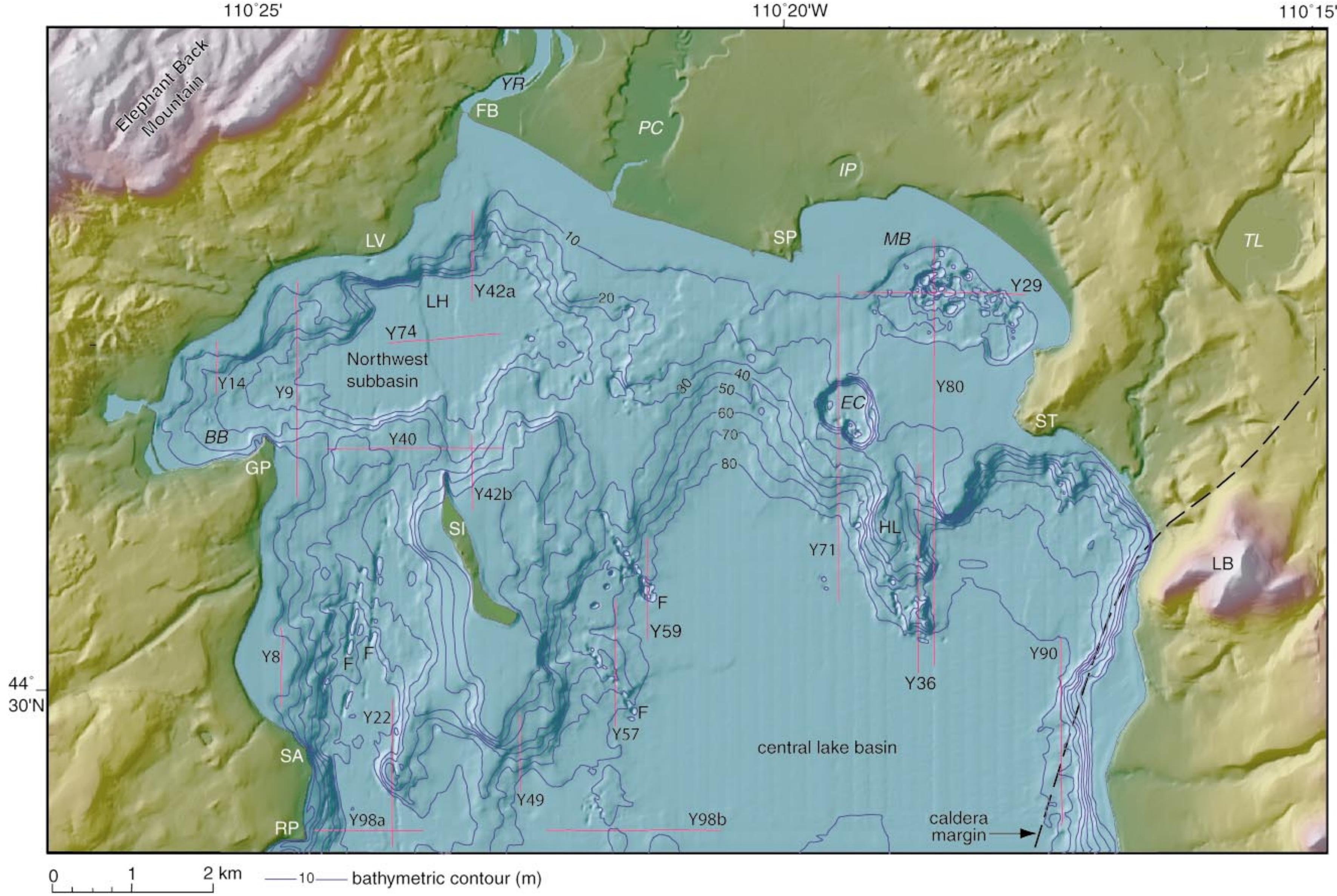

Figure 3. Merged multibeam bathymetric and topographic digital elevation model for northern Yellowstone lake area (prepared by Michael Webring and Greg Lee of the U.S. Geological Survey), showing locations of selected seismic reflection profiles shown in Figures 4–14 and 16–22. Location of caldera margin from Finn and Morgan (2002). South ends of fissures marked by F labels. BB—Bridge Bay; EC—Elliott's crater; FB—Fishing Bridge; GP—Gull Point; HL—hummocky lobe extending south-southeast from Elliott's crater; IP—Indian Pond; LB—Lake Butte; LH—Lake Hotel fault zone; LV—Lake Village; MB—Mary Bay; PC—Pelican Creek; RP—Rock Point; SA—Sand Point; SI—Stevenson Island; SP—Storm Point; ST—Steamboat Point; TL—Turbid Lake; YR—Yellowstone River.

shore (Figs. 1, 3). Lake level is controlled by the elevation of a bedrock spillway at Le Hardy Rapids, 5 km north of the lake (Hamilton, 1987; Pierce et al., 1993, 2002).

Local climate is dominated by heavy winter snowfall and hot dry summers, which cause lake level to fluctuate as much as 1.5 to 1.8 m/yr (Benson, 1961). The lake is dimictic, developing stratified epilimnion, metalimnion, and hypolimnion during summer and winter, and overturning in the autumn and spring. Phytoplankton are primarily diatoms.

SEISMIC REFLECTION DATA

For this investigation, ~450 km of high-resolution seismic reflection profiles were collected concurrently with multibeam bathymetric data in the northern part of Yellowstone Lake (Figs. 2, 3). Track lines were laid out at 200 m spacing on a north-south grid (54 lines) to provide overlapping coverage for compiling the bathymetric data. Seismic reflection and bathymetric data were also collected on nine west- to southwest-trending tie lines and on five shallow-water lines roughly parallel to the coastline.

Seismic reflection data were acquired by using an Edgetech SB-216S tow-fish source and a Triton Elics Delph seismic system. The source generated a 2 kW output pulse with a bandwidth of 2000 to 10,000 Hz. Record lengths of these data were either 150 or 200 ms, depending on water depth, with a sample rate of 0.04 ms. The dominant recorded signal bandwidth of these data is between 2000 and 5000 Hz. Processing consisted of (1) data reformatting, (2) trace-amplitude debiasing (subtracting mean amplitude from trace samples), and (3) automatic gain correction using a 0.88 ms gain window.

Vertical resolution of features imaged on seismic reflection data is ~10 cm. Horizontal resolution, as measured by the source-pulse footprint (partly a function of frequency bandwidth and beam width), is typically 3 m at 10 m water depth and 13 m at 50 m water depth. Maximum signal penetration through lacustrine sediments is ~25–30 ms (~18–23 m), generally on profiles crossing the deepest basinal parts of the lake. Coring results of prior investigations (see next section) indicate that lacustrine sediments consist mainly of semiconsolidated diatomaceous mud, for which we assume velocities of 1500 m/s.

Previously, Otis et al. (1977) collected data on three north-trending and two west-trending seismic reflection lines in northern Yellowstone Lake by using a lower-frequency 1 in.^{3} (16.4 cm^3) airgun source. Their investigation provides important images of the upper ~200 m of the lake subsurface, but lacks the resolution in the upper ~20 m of the subsurface provided by our survey. Tiller (1995) showed four short higher-resolution (comparable to this investigation) seismic reflection profiles over selected coring sites from the South Arm, West Thumb, and central part of Yellowstone Lake (Fig. 1).

SEDIMENTARY FEATURES AND DEPOSITS

Laminated Deep-Basin Deposits

Several seismic reflection profiles show that parts of the deep central basin of Yellowstone Lake (Fig. 3); line Y98b (Fig. 4) provides the most representative image of deep-basinal strata. This profile reveals two seismic sequences. The upper sequence (II) forms a sheet that is typically ~15–22 m (20–30 ms) thick and is characterized by moderate- to high-amplitude, high-frequency, parallel, continuous, and horizontal reflections. The lower sequence (I) comprises low-amplitude, moderate-frequency, subparallel to chaotic, discontinuous reflections. However, the seismic reflection characteristics of sequence I are somewhat obscure because it occurs near the lower limit of signal penetration, generally about ~20 ms below the lake floor. The contact between the two sequences is parallel and conformable.

Coring investigations from other deep parts of the lake (Shero, 1977; Shuey et al., 1977; Tiller, 1995) indicate that the upper ~9 m of these strata consist of variably laminated and mottled diatomaceous mud. Tiller (1995) documented the presence of middle Holocene Mazama ash (7627 ± 150 cal. yr B.P.; Bacon, 1983; Hallett et al., 1997; Zdanowicz et al., 1999) in three cores of basinal sediments from Yellowstone Lake (Fig. 1). He also discovered Glacier Peak ash (~13,400 cal yr B.P.; Foit et al., 1993; Pierce et al., 2002) near the bottom of an 8.6-m-long core between Frank and Dot Islands, ~3.5 km south of our study area (Figs. 1, 2). The presence of these ashes, several ^{14}C dates, and lithologic correlations with the additional cores, indicate basinal sedimentation rates of ~60–100 cm/1000 yr for the past 13,000 yr. At these rates, the Holocene section of the past 10,000 yr is ~6–10 m thick.

Stratified deposits in sequence I below the Holocene section consist of more clastic-rich glaciolacustrine and early postglacial lacustrine silt and clay, for which sedimentation rates should be considerably higher. Such de-

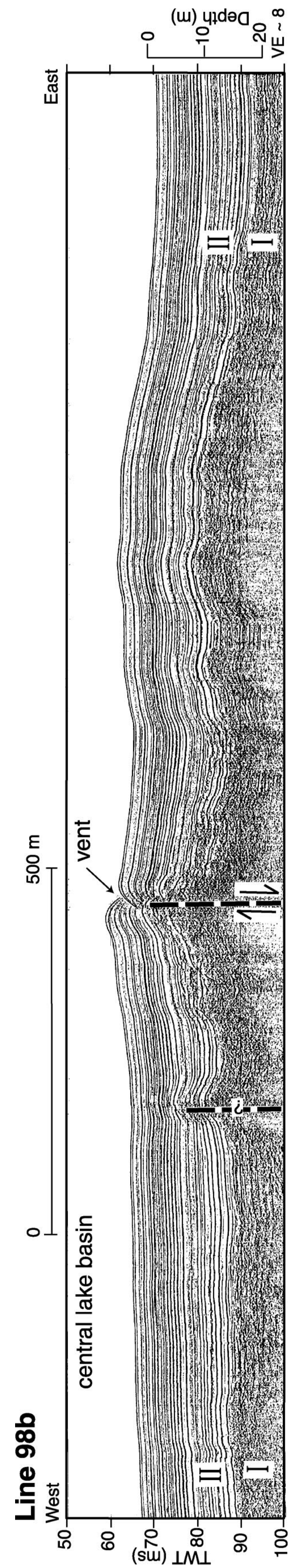

Figure 4. High-resolution seismic reflection profile Y98b from the central lake basin of northern Yellowstone Lake (Fig. 3). I and II represent seismic sequences described in text. Heavy bold lines show faults. The top of the profile is at 50 ms. TWT—two-way traveltime.

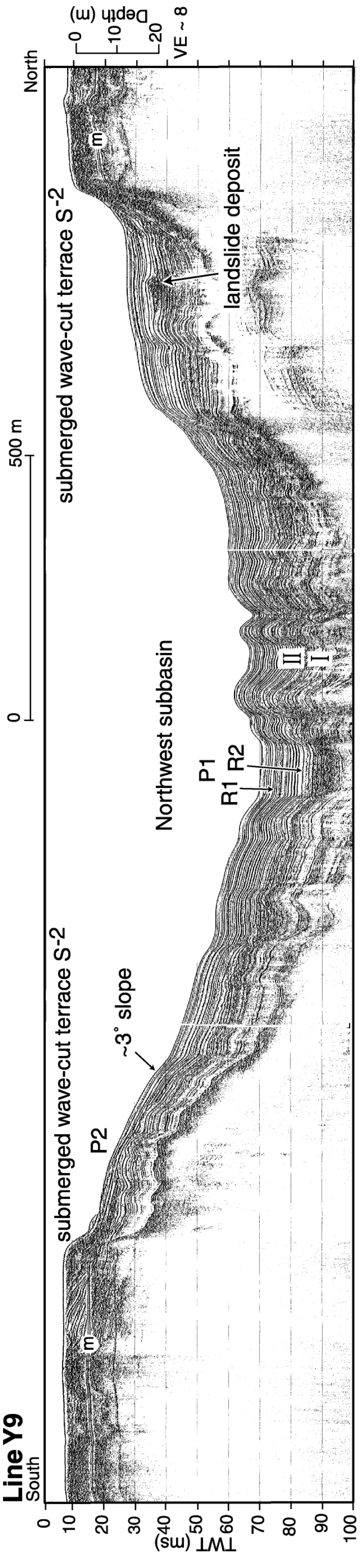

Figure 5. High-resolution seismic reflection profile Y9 crossing the northwest subbasin of northern Yellowstone Lake (Fig. 3). I and II represent seismic sequences, P1 and P2 are locations, and R1 and R2 are distinctive reflections explained in text. TWT—two-way traveltime; m—water-bottom multiple.

posits are well exposed in beach-cliff outcrops between Bridge Bay and Lake Village (Fig. 2; Richmond, 1977a) and were deposited at lake levels ≥20 m higher than today.

Within the central lake basin (Fig. 3), the dense grid of seismic reflection data (Fig. 2) provides the basis for accurate stratigraphic correlation. The vertical sequence of reflections in the upper 10–20 ms (7–15 m) within sequence II is also similar between the deep central lake basin and the northwest subbasin (Figs. 3, 5), consistent with a post–10 ka history in which lake sedimentation has been predominantly of biogenic pelagic origin.

Slope Deposits

Slopes connect the central and northwest subbasin of northern Yellowstone Lake with the shallow terraces that rim the lake and Stevenson Island (Fig. 2). Where not disrupted by landsliding, these slopes typically have dips of 3°–7° and are underlain by strata that yield moderate- to high-amplitude, high-frequency, subparallel reflections that are continuous with those in the subbasins (e.g., Figs. 5, 6). This continuity indicates that they similarly consist of variably laminated and mottled diatomaceous mud.

The ''packages'' of slope reflections typically thin upslope by gentle onlap and internal lensing or pinchout. On line Y49 south of Stevenson Island (Figs. 3, 6), for example, the section between basinal reflections R1 and R2 thins upslope, between locations P1 and P2, from 3.8 m to 0.5 m. On line Y9 crossing Bridge Bay (Figs. 3, 5), strata underlying the slope between the R1 and R2 reflections thin from 6.7 m in the basin at P1 to 1.4 m at inflection point P2 on the slope. This thinning indicates that there has been some reworking and downslope redeposition of diatomaceous mud and/or that sedimentation rates increase with water depth owing to sediment focusing or greater diatom productivity in deeper water.

Landslide Deposits

Bathymetric data (Fig. 3) reveal several locations along the lake margins characterized by an undulating ''scalloped'' shelf edge and irregular hummocky relief at the base of the slope. Seismic reflection data (Figs. 7, 8, 9) reveal that these hummocks are internally characterized by chaotic reflections or are ''reflection free'' (Mitchum et al., 1977). Together, these observations indicate that the hummocky terrane formed by landsliding. Profiles both parallel (Fig. 8) and perpendicular to (Figs. 7, 9) lake margins indicate that landslide deposits vary in thickness from a few tens of centimeters to as much as 10 m and extend as far as 500 m from the base of the slope into the adjacent basin. Landslide debris is commonly draped by basinal lacustrine deposits that thin over the crests of hummocks, resulting in upward-diminishing relief.

The thickness of the sediment that drapes landslide deposits and the estimates of basin sedimentation rates already described provide a rough indication of the age of slope failure. Line Y42a (Fig. 9), for example, shows the thick (~10 m) toe of a landslide with no apparent drape of lacustrine strata, suggesting that the landslide deposit is relatively young (<1000 yr old?). The thinner (~50–500 cm) landslide deposits of line Y98a (Fig. 5) are overlain by 1–2 m of lacustrine deposits, suggesting an age of ca. 3 to 1 ka. Landslide deposits underlying the hummocky terrane of line Y90 (Fig. 8) are locally overlain by as much as 9 m of stratified basinal deposits. At maximum estimated sediment accumulation rates of 100 cm/1000 yr (see previous section, Laminated Deep-Basin Deposits), this thickness indicates that some of the postglacial landslide deposits imaged on Y90 (Fig. 8) are older than 9 ka.

Shallow-Water Deposits and Submerged Shoreline Terraces

The submerged shallow (depth < 15–20 m) margins of northern Yellowstone Lake are generally underlain by relatively flat to very gently dipping terraces. Seismic reflection profiles (Fig. 3) crossing shallow parts of the lake typically image one to four of these terraces at varying depths (e.g., Fig. 10). Slopes on these terraces vary from ~0° to 0.6°.

Seismic reflection profiles reveal that the lacustrine deposits underlying the shallow-water terraces have typically been reworked and either eroded or redeposited. Figure 11 shows part of profile Y8, parallel to the lake shoreline north of Sand Point (Fig. 3). Strata beneath the flat, shallow (10 ms; 7.5 m) terrace yield moderate-amplitude, high-frequency, semicontinuous, low-angle reflections that are

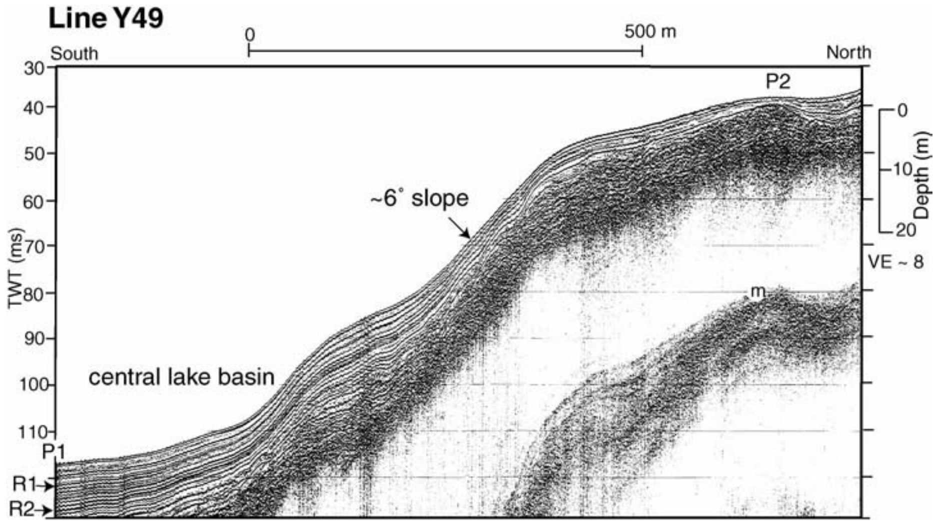

Figure 6. High-resolution seismic reflection profile Y49 from northern Yellowstone Lake south of Stevenson Island (Fig. 3). P1 and P2 are locations, and R1 and R2 are distinctive reflections explained in text. The top of the display is at 30 ms. TWT—two-way traveltime.

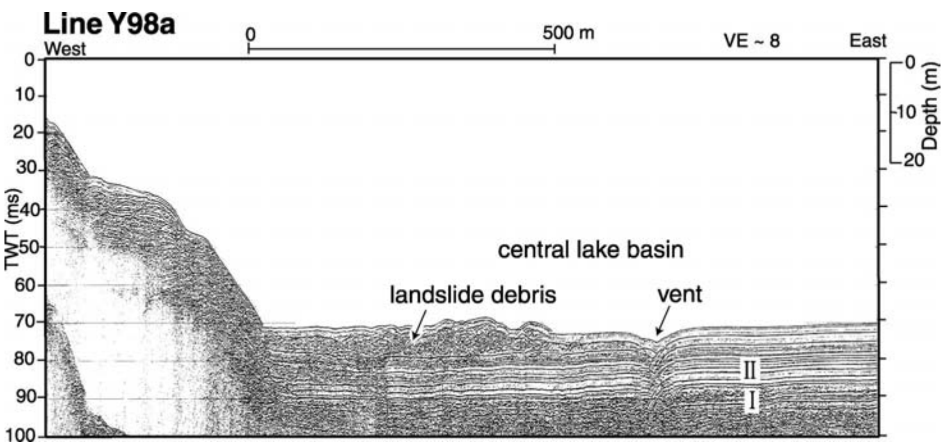

Figure 7. High-resolution seismic reflection profile Y98a from northern Yellowstone Lake offshore of Rock Point (Fig. 3). I and II represent seismic sequences described in text. TWT—two-way traveltime.

erosionally truncated at the lake floor. These strata are probably fine-grained silt and mud that were deposited when the lake level was higher, then eroded and beveled by wave action when the lake level was lower than that of today. Some of the eroded sediment was redeposited as a bar at the south end of the terrace. Figure 12 (line Y14) shows a profile normal to the lake margin that reveals a similar erosional unconformity on a deeper terrace (19 ms; 14 m).

In contrast, many shallow-water terraces such as those displayed on Figures 5, 9, 10, 12, and 13 are underlain by strata that yield chaotic reflections, suggesting that (1) postglacial lacustrine and possibly hydrothermal explosion deposits (see next section) have been reworked by waves and redeposited as a more mixed, poorly stratified, and possibly more coarse-grained deposit, (2) lacustrine deposits have been completely eroded and the shallow substrate consists of massive Pleistocene glacial deposits, and/or (3) terrace sedi-

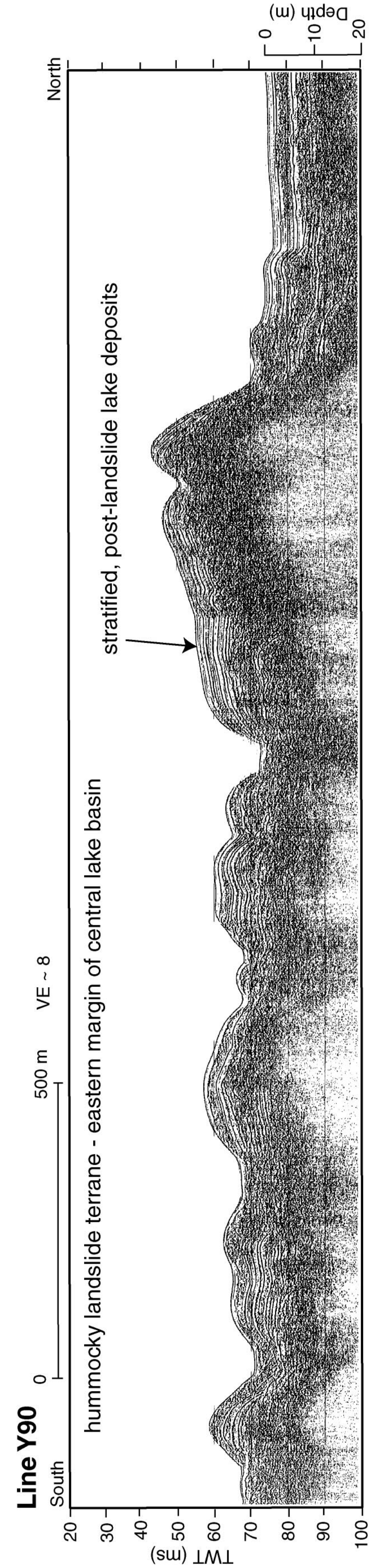

Figure 8. High-resolution seismic reflection profile Y90 from the eastern margin of the central lake basin, northern Yellowstone Lake (Fig. 3). The top of the display is at 20 ms. TWT—two-way traveltime.

ments are gas charged (e.g., Fader, 1997) and/or hydrothermally altered.

On many profiles, the shallow-water terraces are bounded up-dip by scarps or inflection points of inferred wave-erosional origin (e.g., Figs. 10, 12, 14). The intersection of the terrace and the slope defines the ''shoreline angle,'' commonly used in studies of marine terraces as the best marker of water level at the time of terrace formation (e.g., Bradley and Griggs, 1976).

Many of the terraces are bounded basinward by terrace bars (e.g., Figs. 11, 12) formed by wave erosion and redeposition of shoreline sediment. These bars are commonly wedge shaped, overlie a planar erosion surface, range in thickness from ~30 to 300 cm, are as wide as ~100 m, and are typically graded to the elevation of the adjacent terrace flat. Internally, some are characterized by chaotic reflections or are reflection-free, and others are characterized by flat to gently dipping, discontinuous, moderate-amplitude reflections.

Meyer and Locke (1986), Locke and Meyer (1994), and Pierce et al. (2002) used the elevations of shoreline angles and the crests of terrace bars to document lake-level change and vertical deformation around Yellowstone Lake. By using the depths of these same two indicators as well as the depth of shallow, broad terraces, we document four submerged shorelines beneath northern Yellowstone Lake. The estimated depths and correlations of the four submerged shoreline terraces are shown in Figure 15. The depths are relative to the ''0'' height on the lake-level gauge at Bridge Bay, the datum also used in investigations of the emergent terraces. The mean elevation of the modern shoreline angle is 1.80 m above the gauge datum (Locke and Meyer, 1994). Lake level was high at the time of our 1999 survey, ranging from 1.85 to 1.95 m above the datum.

Correlation of terraces was based primarily on their continuity determined from shore-parallel seismic reflection profiles and bathymetric data (Fig. 3). For the emergent terraces surrounding Yellowstone Lake, Locke and Meyer (1994) indicated uncertainty of ~0.5 m in their elevation estimates because of post-abandonment slope and other degradational processes. Our estimates have larger uncertainties (±100 cm?) because of observed local variability in depth for the three indicators (shoreline angle, terrace flat, bar crest) on any one paleoshoreline terrace, common gentle lakeward terrace dips, and the varied angles at which seismic reflection profiles intersect the different terraces. Some seismic reflection profiles (e.g., lines Y29 and Y80; Figs. 13, 16) show submerged wave-cut terraces that merge with no obvious bathymetric break; data from these ''composite shoreline terraces'' are not used in the analysis of Figure 15.

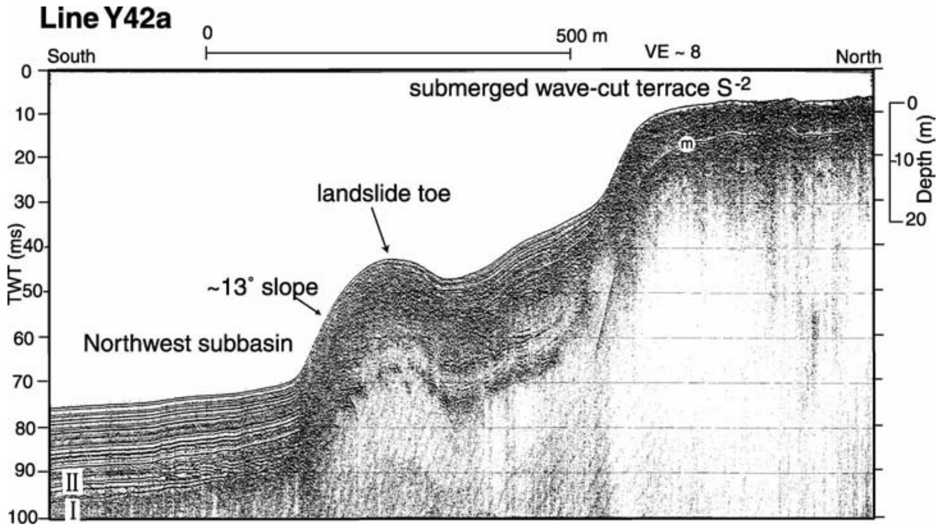

Figure 9. High-resolution seismic reflection profile Y42a from northern Yellowstone Lake south of Fishing Bridge (Fig. 3). I and II represent seismic sequences described in text. TWT—two-way traveltime; m—water-bottom multiple.

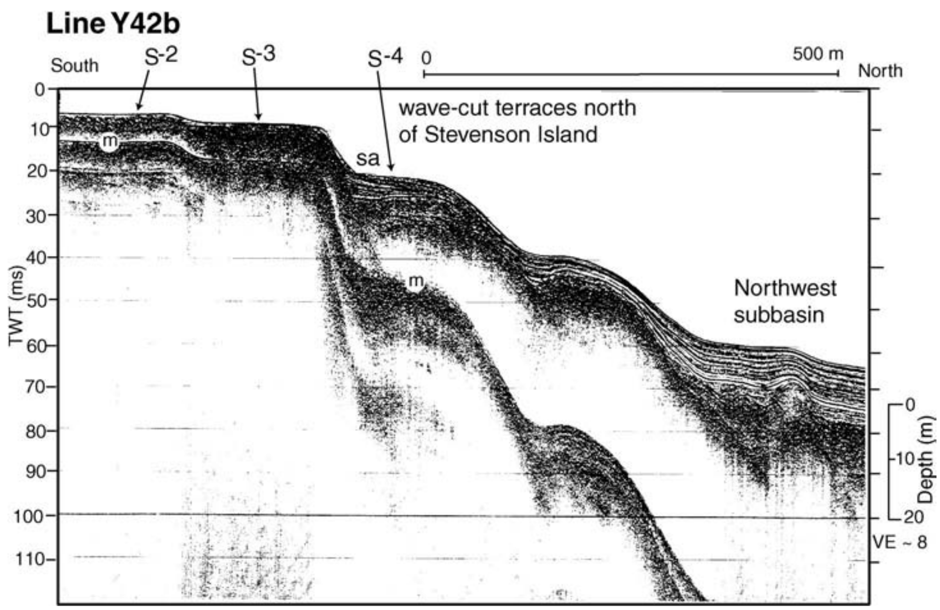

Figure 10. High-resolution seismic reflection profile Y42b from northern Yellowstone Lake, north-northeast of Stevenson Island (Fig. 3). TWT—two-way traveltime; sa—shoreline angle; m—water-bottom multiple.

The depth of the shallowest submerged terrace (S^{-1}), ~10 to 70 cm below datum, was determined mainly on the basis of the crests of terrace bars. This surface is ~1.9 to 2.6 m below the modern shoreline angle (Locke and Meyer, 1994). We recognized this terrace primarily near Fishing Bridge (Fig. 15), but it must be more extensive—our imaging of S^{-1} was limited by shallow water. Available data are insufficient to determine tilting or deformation of this surface.

Shoreline terrace S^{-2} is the most prominent and widespread submerged shoreline terrace, occurring at depths that range from ~2 to 4 m below datum (Fig. 15). The shallowest depths occur along the northeastern shore of the lake between Fishing Bridge and Mary Bay; the greatest depths for this shoreline are

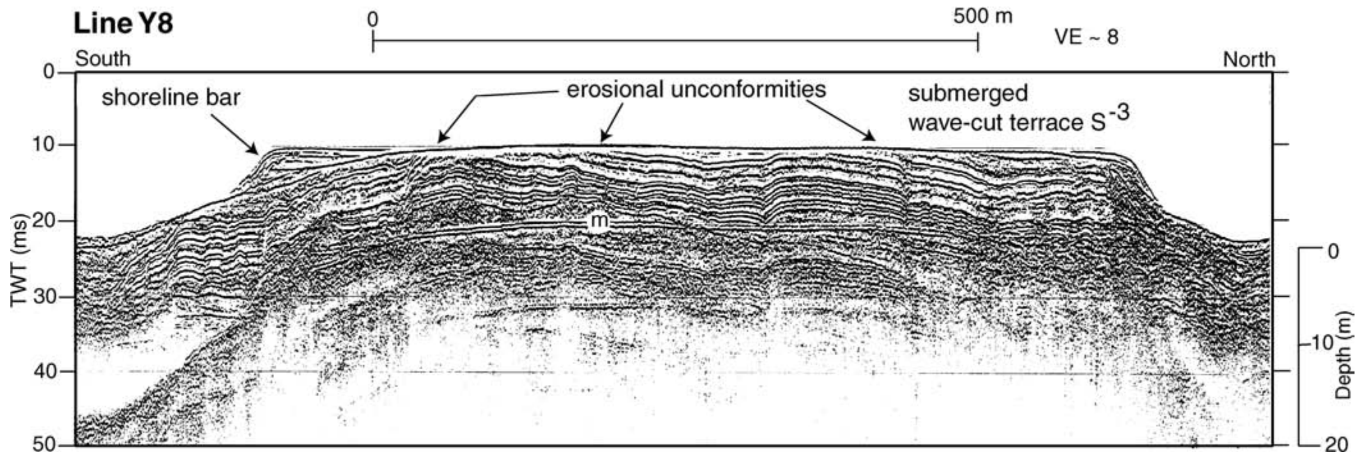

Figure 11. High-resolution seismic reflection profile Y8 from northern Yellowstone Lake, north of Sand Point (Fig. 3). TWT—two-way traveltime; m—water-bottom multiple.

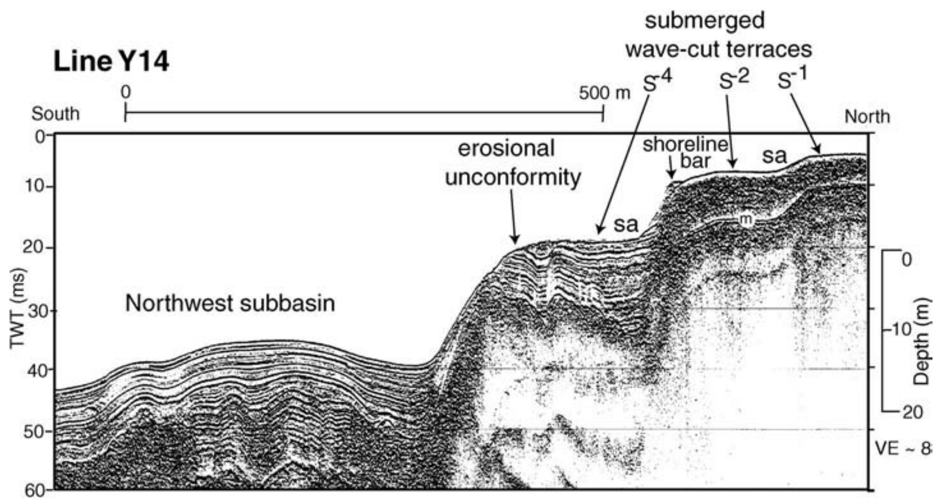

Figure 12. High-resolution seismic reflection profile Y14 from the northwest flank of Bridge Bay, northern Yellowstone Lake (Fig. 3). TWT—two-way traveltime; sa—shoreline angle; m—water-bottom multiple.

south of Steamboat Point along the east coast of the lake. Submerged terrace S^{-2} forms much of the broad platform imaged between Elliott's crater and Steamboat Point (Figs. 3, 13, 14).

Shoreline terrace S^{-3} occurs at depths of ~5–8(?) m and is best revealed in the northwestern part of the lake between Sand Point and Bridge Bay and off the northern coast of Stevenson Island. Along the north and east shores of Yellowstone Lake, the discontinuity of the terrace suggests that it has been significantly eroded. Remnants of this terrace are present offshore of Fishing Bridge and between Mary Bay and Lake Butte to the east (Fig. 15). Part of the broad platform between Elliott's crater and Steamboat Point (Fig. 3) is underlain by the S^{-3} terrace.

Shoreline terrace S^{-4} varies in depth from ~9 to 13 m and is best expressed offshore of northern Stevenson Island and between Bridge Bay and Mary Bay along the northern shore of the lake. This terrace was not recognized south of Mary Bay along the eastern shore of the lake, the site of extensive landsliding (Figs. 3, 8). Several well-developed S^{-4} shoreline angles on adjacent seismic reflection profiles differ in depth by as much as 1 m, suggesting local tilting or offset. Elevation measurements of emergent shoreline terraces commonly show similar local variation in elevation (Meyer and Locke, 1986; Locke and Meyer, 1994; Pierce et al., 2002).

The four submerged terraces recognized in this study match four of the seven submerged terraces (L1 to L7) that were informally described by Hamilton and Bailey (1988, 1990) in northern Yellowstone Lake. S^{-1}, S^{-2}, S^{-3}, and S^{-4} correlate with L1, L2, L3, and L5, respectively. We did not recognize the L4, L6, or L7 submerged shorelines of Hamilton and Bailey (1990), which may be present but could not be confirmed with our data set.

HYDROTHERMAL FEATURES AND DEPOSITS

Hydrothermal Explosion Craters

Mary Bay Crater

Wold et al. (1977) and Kaplinski (1991) documented the presence of a submerged hydrothermal crater at Mary Bay (Fig. 3) on the basis of bathymetric data and magnetic profiling. The crater continues to be the site of geothermal activity, characterized by extremely high heat flow (Morgan et al., 1977). On land to the north and east of Mary Bay, Richmond (1977a, 1977b) mapped a band of hydrothermal explosion breccia correlated with the Mary Bay crater as far as 4 km from the lake margin. Pierce et al. (2002) dated these deposits as ca. 13 ka.

New high-resolution seismic reflection and bathymetric data (Figs. 3, 13, 16) show that the oval-shaped Mary Bay crater is ~2000 m long and 1300 m wide; it has a surface area of ~1.7 km^2 and a maximum depth of ~45 m (60 ms). The volume (the void between the crater rim and floor) of this crater is ~20×10^6 m^3; however, the original crater was probably larger (Wold et al., 1977). The original morphology of the explosion crater has been modified by lacustrine erosion and redeposition associated with Holocene lake-level fluctuations and overall decline. There is no longer a well-defined crater rim in the lake, and

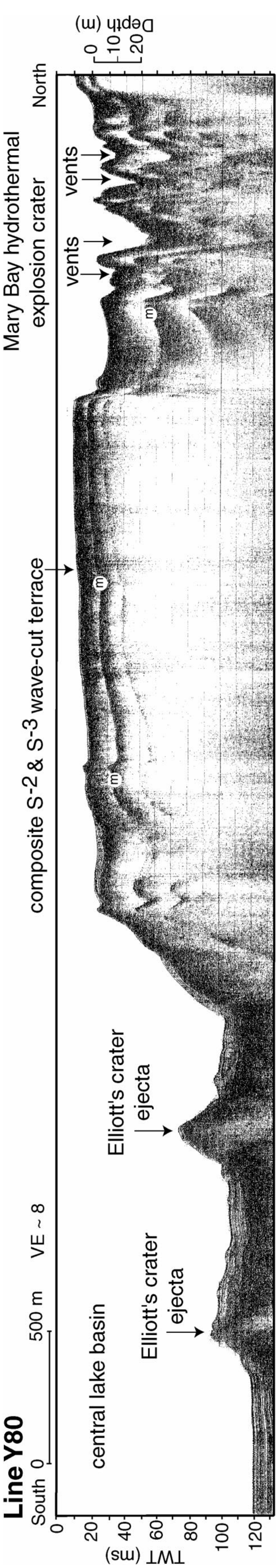

Figure 13. High-resolution seismic reflection profile Y80 extending from Mary Bay to the central lake basin in northern Yellowstone Lake (Fig. 3). TWT—two-way traveltime; m—water-bottom multiple.

crater ejecta deposits appear to have been reworked to form the broad submerged terrace that surrounds Mary Bay (Figs. 3, 13, 14).

The floor of the crater is occupied by a large number of smaller craters and hydrothermal vents and domes of various sizes (Figs. 3, 13, 16). For example, west-trending line Y29 (Fig. 16) imaged at least 20 relatively sharp V-shaped depressions in the floor of the crater that represent active or recently active vents. North-trending line Y80 (Fig. 13) imaged at least 10 of these crater-floor depressions. The irregularity of the crater floor supports the hypothesis that the crater has a composite origin, formed by two or more explosions within a relatively short time interval. A composite origin helps explain the anomalously large size of the Mary Bay crater compared to other hydrothermal explosion craters (Browne and Lawless, 2001).

Given that the crater complex formed at ca. 13 ka, strata beneath the crater floor probably consist of massive breccia and lake deposits of latest Pleistocene age overlain by Holocene lake deposits. The strata that comprise the crater floor are characterized by chaotic reflections, probably due to significant gas content and/or hydrothermal alteration.

Elliott's Crater

Elliott's crater occurs southwest of the Mary Bay crater in northeastern Yellowstone Lake (Figs. 3, 14). The northern part of the crater is roughly circular, and there is a prominent south-southeast–trending embayment on its south-southeast flank. Elliott's crater has a diameter of ~700 m, a surface area of ~0.35 km², a maximum depth of ~64 m (85 ms), and a volume (the void between the crater rim and floor) of ~12 × 10⁶ m³. The original morphology of the crater is preserved because it formed at water depths below the effects of shoreline processes.

Postexplosion lacustrine strata within the crater are characterized by moderate- to high-amplitude, continuous, parallel reflections (Fig. 14) similar to those found in the lake's deep basins (see section on Laminated Deep-Basin Deposits). Recent hydrothermal activity is confined to vents on the southern margin of the crater floor. Parallel reflections in the

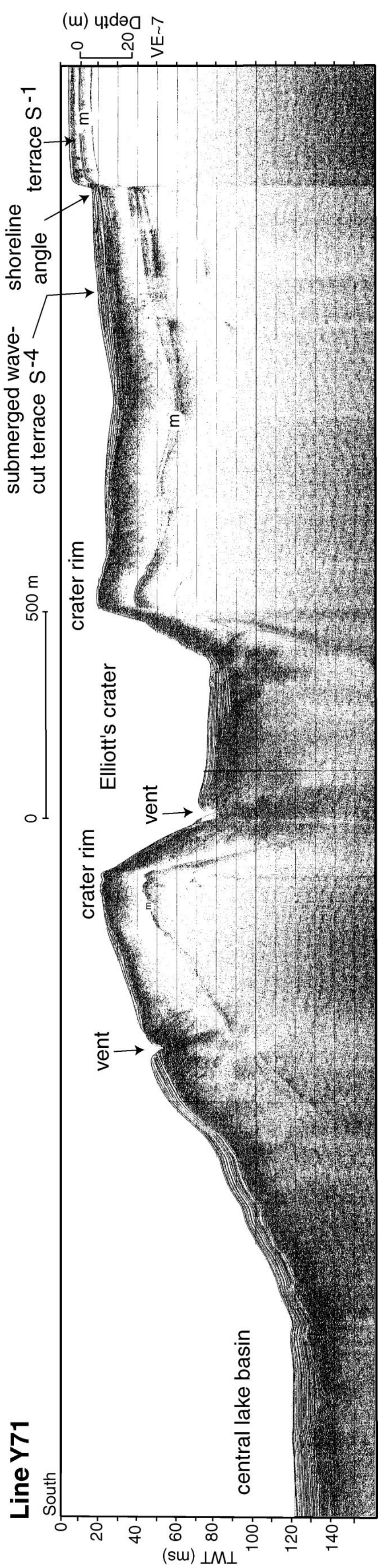

Figure 14. High-resolution seismic reflection profile Y71 from northern Yellowstone Lake, extending from Mary Bay across Elliott's crater to the central lake basin (Fig. 3). TWT—two-way traveltime; m—water-bottom multiple.

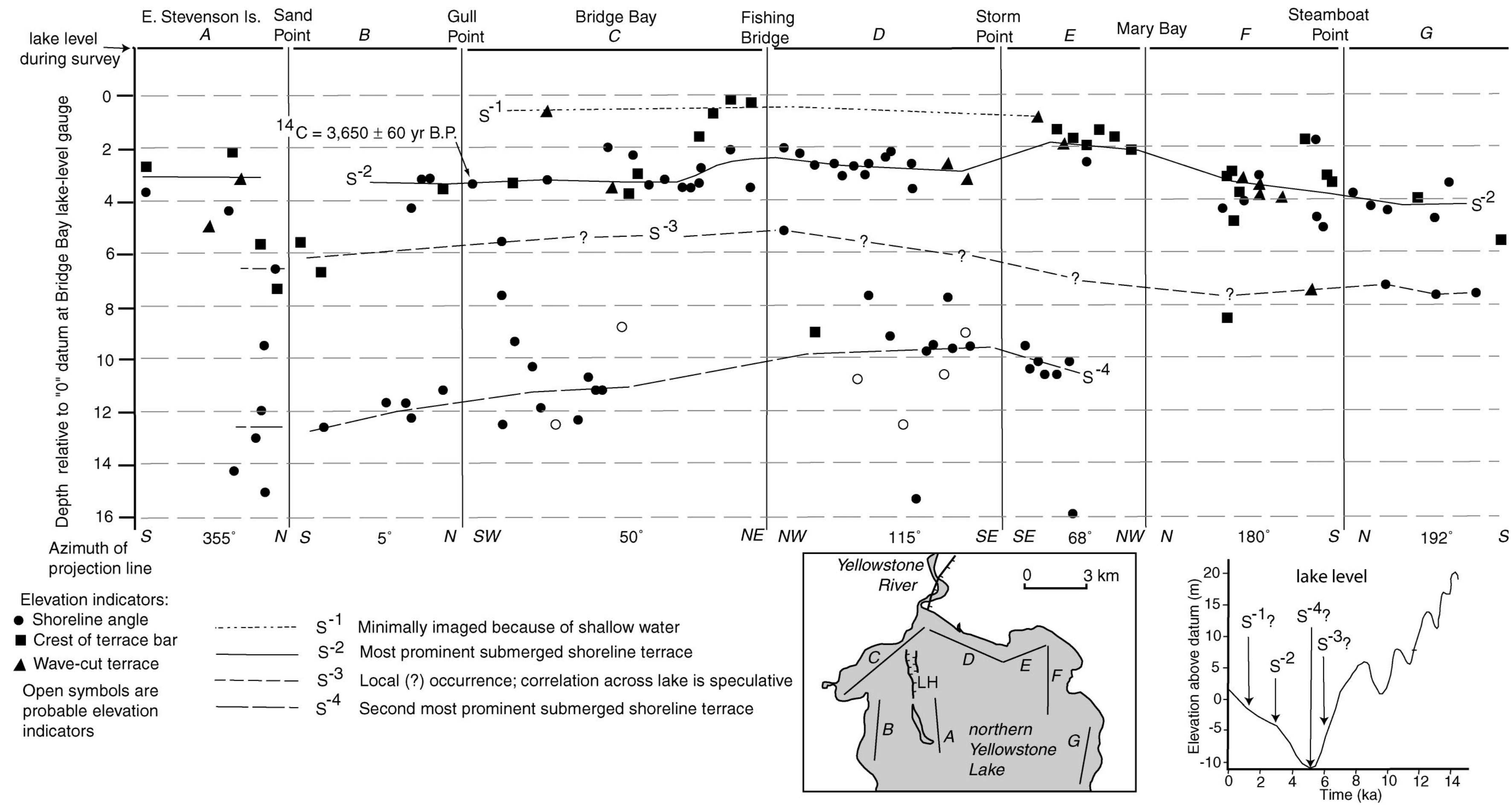

Figure 15. Elevations of submerged shoreline terraces around northern Yellowstone Lake. LH—Lake Hotel fault zone. Location of normal fault at lake outlet is from Pierce et al. (2002). Ticks are on downthrown side of faults. Radiocarbon date (near Gull Point) is from wood in submerged beach sands and gravels. Lake-level curve is from Pierce et al. (2002) except for between 7 and 3 ka (see text for explanation).

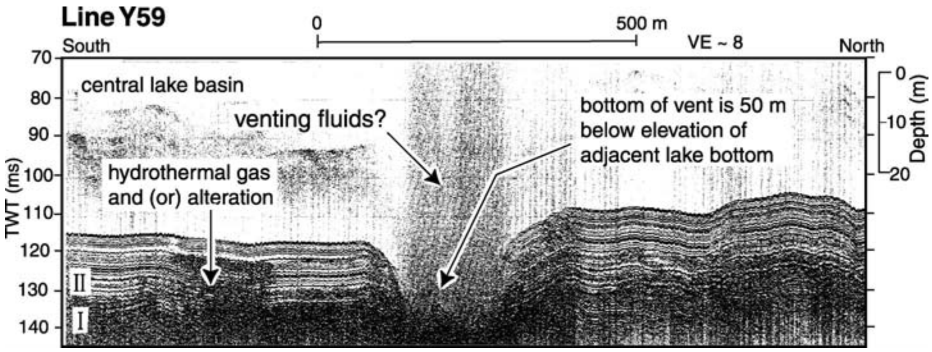

Figure 17. High-resolution seismic reflection profile Y59 from the west flank of the central lake basin, northern Yellowstone Lake (Fig. 3). I and II represent seismic sequences described in text. The top of the profile is at 70 ms. TWT—two-way traveltime.

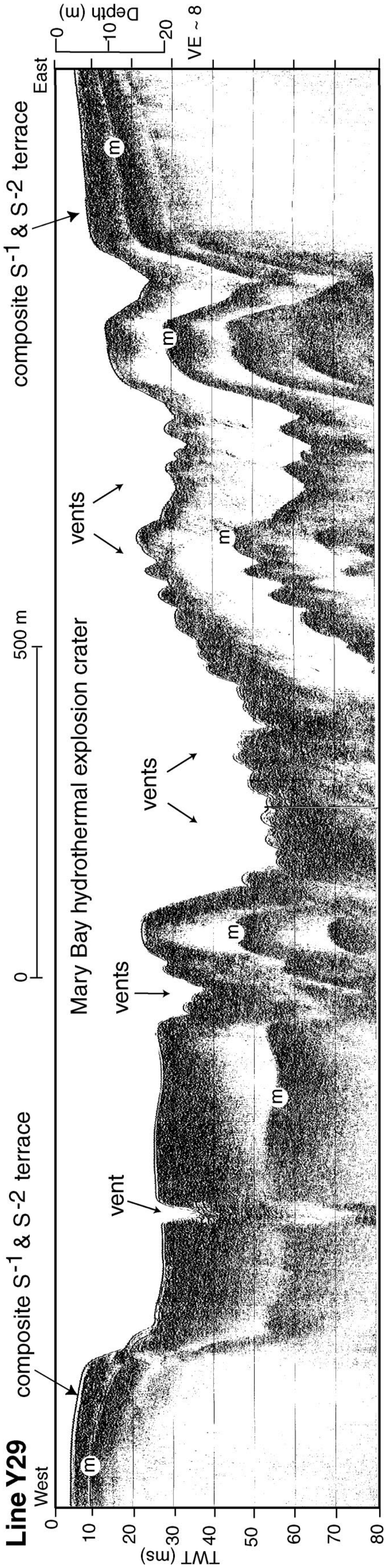

Figure 16. High-resolution seismic reflection profile Y29, crossing Mary Bay in northern Yellowstone Lake (Fig. 3). TWT—two-way traveltime; m—water-bottom multiple.

crater-floor deposits grade laterally into a zone of chaotic reflections proximal to these vents, presumably resulting from increasing hydrothermal gas content or alteration.

The origin of Elliott's crater postdates Pinedale glaciation (ca. 16 ka) and can be further constrained by using the thickness of the post-explosion sediment fill (11 ms, ~8 m) and the basinal sediment-accumulation rates (60–100 cm/1000 yr) previously outlined. With this approach, we interpret that Elliott's crater formed between ca. 13 and 8 ka.

Smaller Crater-Like Basins

New data reveal many smaller circular basins on the lake floor (Figs. 3, 17, 18). Because of their size and the spacing of the track-line grid (Fig. 2), only a few of these were imaged by seismic reflection profiles. Perhaps the largest of these smaller basins (width ~175 m) occurs at the southern end of a fissure zone east of Stevenson Island (Figs. 3, 17). The basin floor has a depth of 133 m, ~50 m below the surrounding lake floor. The temperature of fluids (sampled by ROV [remotely operated vehicle]) venting at this locality is more than 120 °C.

Smaller circular basins have typical diameters of ~20–60 m, depths of 5–15 m, and relatively flat bottoms and are partly filled by flat-lying lacustrine deposits (e.g., Fig. 18). On the basis of their size and shape, it is possible that these basins formed by smaller hydrothermal explosions. However, it is also possible that some formed as large V-shaped hydrothermal vents (see subsequent section Hydrothermal Vents and Domes) and that their flat bottoms result from postventing infill by lacustrine deposits. The lack of an obvious breccia apron surrounding many of these small basins is more consistent with an origin as a hydrothermal vent.

Hydrothermal Explosion Breccia

On land, hydrothermal explosion breccias have been mapped around the east and north flanks of the subaqueous Mary Bay crater and also surround the Turbid Lake and Indian Pond hydrothermal explosion craters (Fig. 3; Richmond, 1977a, 1977b). Similar deposits must also occur on the floor of Yellowstone Lake, most notably beneath the shallow (<15 m) subaqueous shelf area surrounding the Mary Bay crater (Fig. 3). Strata beneath this shelf area are characterized by chaotic reflections (Figs. 13, 14, 16), consistent with the rapid mode of emplacement, lack of stratification, and poor sorting that are characteristic of explosion breccia. Following deposition, these strata were beveled by shoreline processes at the time that the submerged shoreline terraces formed (Fig. 15).

On the basis of similar reflection characteristics, irregular hummocky relief, and alignment with the crater embayment (Fig. 3, see) we infer that significant hydrothermal explosion breccia also forms the upper part of the lobe that extends south-southeast from Elliott's crater (Figs. 3, 13, 19). Mounds of sediment, characterized by chaotic reflections, are variably draped by younger basinal lacustrine deposits causing the irregular relief on the lobe. The draped mounds resemble those formed by landslides (e.g., Fig. 8). However, they occur as much as 1700 m away from the closest shallow-water terrace (surrounding

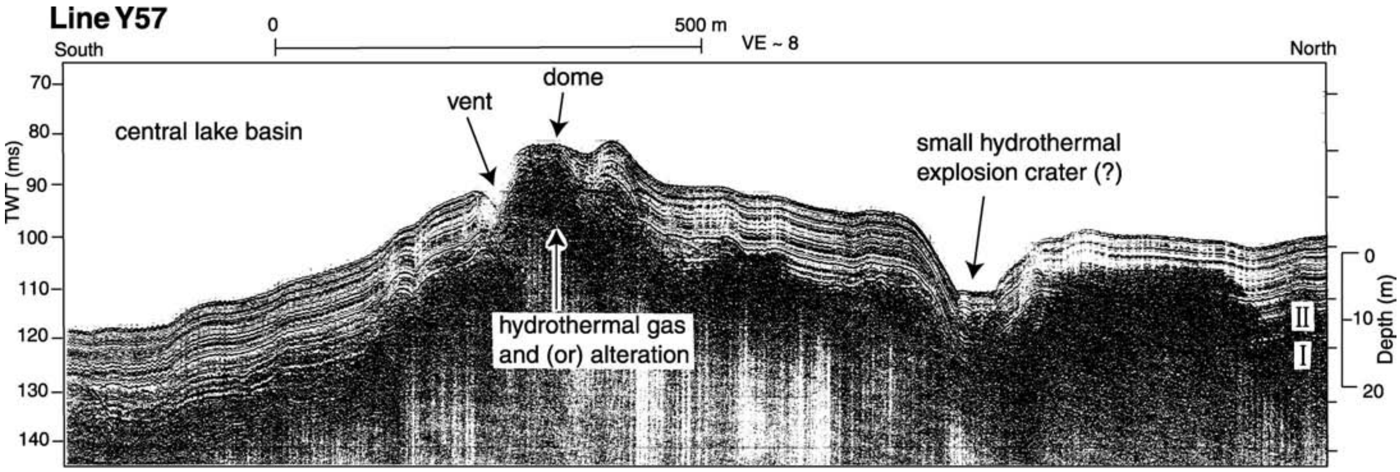

Figure 18. High-resolution seismic reflection profile Y57 from the west flank of the central lake basin, northern Yellowstone Lake (Fig. 3). I and II represent seismic sequences described in text. The top of the profile is at 66 ms. TWT—two-way traveltime.

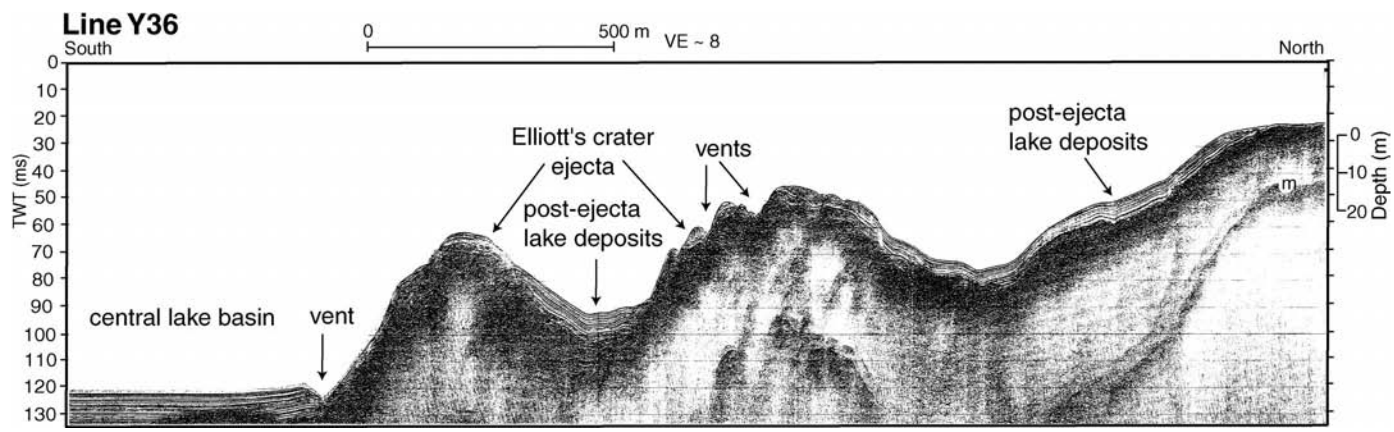

Figure 19. High-resolution seismic reflection profile Y36 from the north flank of the central lake basin, northern Yellowstone Lake (Fig. 3). TWT—two-way traveltime; m—water-bottom multiple.

Mary Bay), two to three times farther than other landslides extend into the basin from the present lake-margin terraces. Primary origin by landsliding is thus unlikely. The maximum thickness of lacustrine sediment preserved between the hummocky breccia mounds (Fig. 18; ~7.5 m) is comparable to that preserved on the floor of Elliott's crater (Fig. 14; ~8 m), consistent with synchronous origin of the crater and the sediment lobe. Although the hummocky lobe (Fig. 3) occupies about twice the surface area of Elliott's crater, the volume of the mounded sediment in the lobe (above a continuous slope from the crater rim to the basin floor) is smaller than the crater volume (see previous crater description). Elliott's crater explosion deposits thus must also occur elsewhere in the lake. Comparable hummocky breccia is not present in deep water directly south, southwest, or west of the crater, indicating markedly asymmetric sediment dispersal. We have also noted asymmetric breccia distribution for the nearby Indian Pond hydrothermal explosion crater (Fig. 3) as did Muffler et al. (1971) for the Twin Buttes hydrothermal explosion crater, which is located ~30 km west of northern Yellowstone Lake. Browne and Lawless (2001) also discussed a directional hydrothermal explosion blast at Waimangu in New Zealand.

Fissure Zones

Three prominent, north-northeast–trending (0°–12°), 2–3-km-long, subparallel, fissure zones occur between Stevenson Island and the western shore of Yellowstone Lake (Fig. 3). Two northwest-trending (~330°), 1–1.3-km-long, fissure zones occur 1–2 km east and southeast of Stevenson Island. An ~1-km-long, north-northwest–trending (~350°) fissure zone cuts the hummocky lobe that extends south-southeast of Elliott's crater. Seismic reflection data indicate that hydrothermal features, including vents and domes (see next section), are concentrated along these fissures.

One of the fissure zones east of Stevenson Island appears to be partly fault controlled. Line Y59 (Fig. 17), which obliquely crosses this zone, shows that the lake floor and underlying distinct reflections of sequence II are ~6.7 m (9 ms) higher northwest of the fissure axis (the deep vent) than on its southeast side. The hypothesis that all of the fissure zones are fault controlled cannot be tested because few of our east-west seismic reflection tie lines cross the fissure zones in optimum locations (Figs. 2, 3). The orientation of these fissure zones is consistent with and may be related to the regional pattern of approximate east-west extension noted for the eastern margin of the

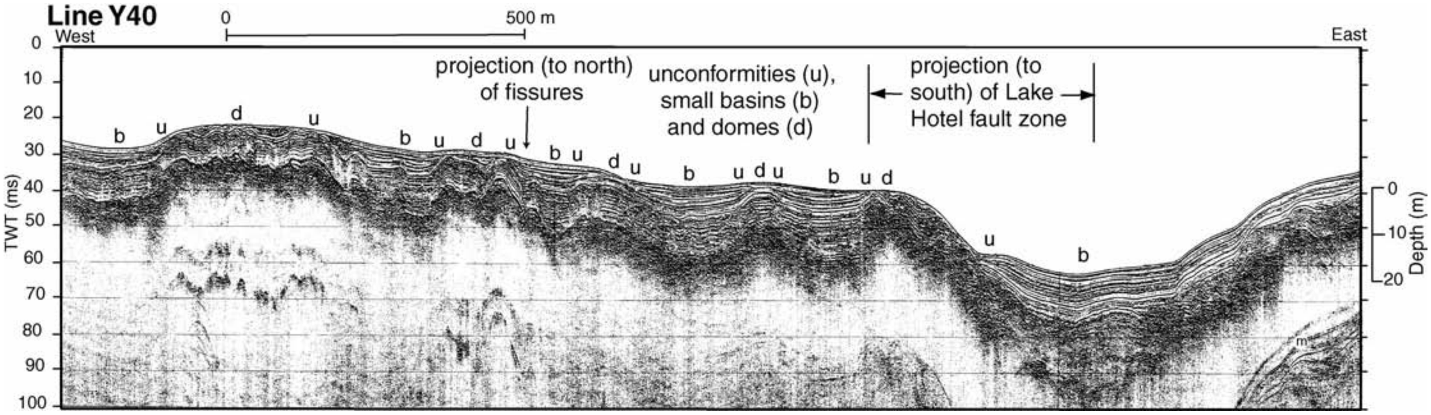

Figure 20. High-resolution seismic reflection profile Y40 from northern Yellowstone Lake, north of Stevenson Island (Fig. 3). TWT—two-way traveltime.

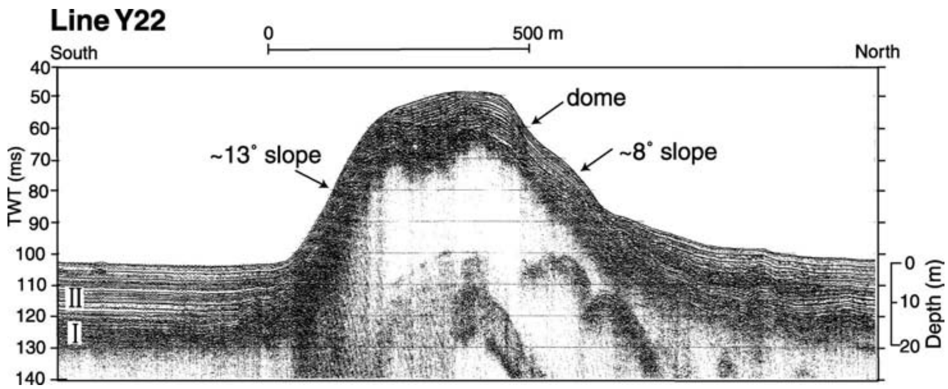

Figure 21. High-resolution seismic reflection profile Y22 from northern Yellowstone Lake, offshore of Sand Point and Rock Point (Fig. 3).). I and II represent seismic sequences described in text. TWT—two-way traveltime.

Basin and Range province (Smith et al., 1977).

Hydrothermal Vents and Domes

Numerous small depressions ($n > 150$; typical diameter $\leq$ 30 m) occupy the floor of northern Yellowstone Lake (Fig. 3). Submersible ROV investigations of many of these depressions indicate that they are hydrothermal vents, with temperatures approaching 120 °C. These vents have wide distribution; their greatest concentration is along linear fissure zones and in the floors of the Mary Bay and Elliott's craters.

The sublacustrine vents typically have a V-shaped morphology, well represented on several vertically exaggerated seismic reflection profiles (Figs. 4, 13, 14, 16, 18). In many cases, vent margins are draped by lacustrine deposits; this geometry suggests either that the vent is old or that it formed by subsurface dissolution of underlying strata, forcing gentle collapse and warping of younger, overlying deposits. In other cases, the truncation of lacustrine strata are truncated along vent margins suggests forceful expulsion of fluids or gases through the vent and/or a relatively young vent age.

The age and activity of a particular vent can be assessed qualitatively by the character of reflections from the lacustrine strata on its flanks, which we correlate with gas content or hydrothermal alteration in the sediment column. In the Mary Bay crater (Figs. 13, 16), for example, shallow sediments characterized by chaotic reflections are consistent with high heat flow (Morgan et al., 1977) and the presence of hydrothermal gas and/or alteration. Other examples of strata with chaotic reflections adjacent to vents occur on the flank of Elliott's crater (Fig. 14) and east of Stevenson Island (Fig. 18). Hydrothermal vents south of Stevenson Island in the deeper, central lake basin (Figs. 4, 7) are bounded by strata characterized by parallel reflections and probably are less active.

Local doming of the lake floor caused by buildup of hydrothermal pressures beneath sealed zones is common in northern Yellowstone Lake. This doming is manifested on seismic reflection profiles by gently warped bathymetry and/or stratigraphy (Figs. 18, 20, 21). For each suspected occurrence of such doming, other processes that can also produce mounded deposits, such as landsliding or ejecta deposition, have been ruled out. Some areas of irregular bathymetry may have compound origins. For example, the hummocky relief inside the Mary Bay crater (Figs. 13, 16), probably results from a combination of doming, deposition of breccia, landslides off the crater margins, and subsurface dissolution.

Most doming of the lake floor appears to occur on a relatively local scale. For example, on line Y40 north of Stevenson Island (Fig. 19), shallow lacustrine strata form numerous domes and basins bounded by unconformities and pinchouts. Dome and basin height (or depth) and width are typically less than ~10 m and 100 m, respectively. Thinning of basin reflections over adjacent domes represents syndepositional dome growth. Y40 crosses the northward projection of the two fissure zones that occur west of Stevenson Island (Fig. 3), and it is likely that subsurface hydrothermal alteration and gas concentration along that trend contribute to this shallow deformation and the variable character of reflections imaged on this profile. The relatively well-preserved stratification in the shallow subsurface and the distance from lake margins and hydrothermal explosion craters argue against landsliding or breccia deposition as the origin of the hummocky stratigraphy on line Y40.

Line Y57 (Fig. 18) obliquely crosses a fis-

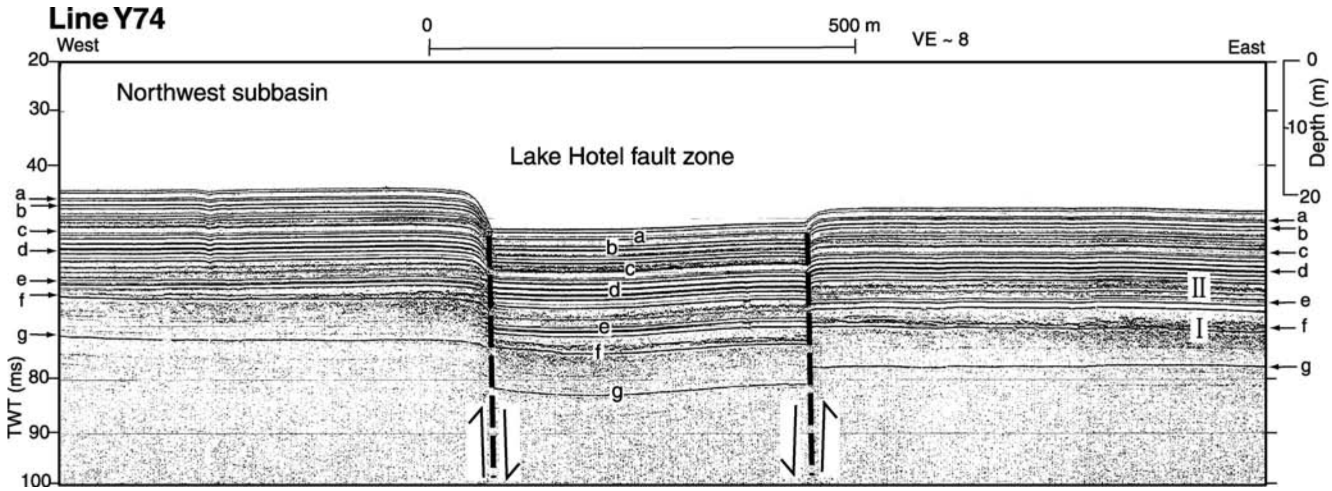

Figure 22. High-resolution seismic reflection profile Y74, crossing the Lake Hotel fault zone in the northwest subbasin of northern Yellowstone Lake (Fig. 3). I and II represent seismic sequences, and labels a–g indicate distinctive reflectors, as described in text. TWT—two-way traveltime.

TABLE 1. MEASURED OFFSETS OF DEPOSITIONAL SURFACES CUT BY THE LAKE HOTEL FAULT ZONE (LINE Y74, FIG. 22) AND INFERRED HISTORY OF FAULT RUPTURE (FIG. 23)

Surface	Western fault (cm)	Eastern fault (cm)	Entire zone (cm)
Lake floor	570	280	290
Event 3			
Reflector a	560	260	300
Reflector b	600	300	300
Event 2			
Reflector c	680	360	320
Reflector d	680	370	310
Reflector e	700	390	310
Event 1			
Reflector f	740	330	410
Reflector g	750	340	410

Offset history:
Event 1: 50 cm offset on western fault, (45) cm offset on eastern fault, 95 cm offset across zone.
Event 2: 90 cm offset on western fault, 75 cm offset on eastern fault, 15 cm offset across zone.
Event 3: 580 cm offset on western fault, 280 cm offset on eastern fault, 300 cm offset across zone.

sure zone east of Stevenson Island in the central lake basin (Fig. 3) and images doming on a larger scale. There is ~28 m of relief over ~600 m distance on the asymmetric bathymetric mound. The presence of a vent at the center of this mound and the chaotic reflections yielded by strata at the core of the mound indicate recent hydrothermal activity. Dome growth, related to buildup of hydrothermal pressures beneath a seal, presumably stopped when those pressures were released by venting.

The largest feature on the lake floor that we tentatively interpret as a dome occurs ~1 km west of Sand Point (line Y22; Fig. 21). This roughly circular feature is anomalously large, ~650 m wide, and has 40 m of relief above the lake floor. Slopes on its northern and southern flanks are 8° and 13°, respectively. The inferred dome has a large vent at its core (not imaged on line Y22). As with line Y57 (Fig. 18), we speculate that hydrothermal pressures warped the lake floor up and were then diminished through venting, effectively ending dome growth and possibly causing some deflation.

Doming comparable in scale and geometry to that displayed on line Y40 (Fig. 20) is common in northern Yellowstone Lake and is of a magnitude similar to that of the deformation of exposed shoreline terraces surrounding the lake (Meyer and Locke, 1986; Locke and Meyer, 1994; Pierce et al., 2002). The amount of relief on the domal features on lines Y57 and Y22 (Figs. 18, 21) is, in contrast, larger than that described on land. This contrast could indicate that either (1) different processes of hydrothermal circulation and dome growth operate in sublacustrine and terrestrial environments, or (2) some of the relief on the larger sublacustrine domes can be attributed to underlying relict glacial landforms or to rhyolitic lava flows.

ACTIVE FAULTS

Lake Hotel Fault Zone

We collected three seismic reflection profiles crossing a north-trending graben between Stevenson Island and Lake Village (Fig. 22). Otis et al. (1977) originally recognized this zone, but their map shows it ~800 to 1000 m east of its location as revealed by our surveys. We informally designate this fault zone the ''Lake Hotel'' fault because of its proximity to the Lake Hotel in Lake Village (Fig. 3). Otis et al. (1977) suggested that the two graben-bounding faults have ''displacements of ~10 m.''

Table 1 and Figure 23 provide information and interpretation of fault offsets based on recognition of distinctive reflectors a through g (Fig. 22). Reflectors f and g occur within largely reflection-free material and represent clastic glaciolacustrine to early postglacial lacustrine deposits (sequence I; see previous description, Laminated Deep-Basin Deposits); the section above reflector f is characterized by high-frequency, moderate- to high-amplitude reflections and consists of diatomaceous mud (sequence II). Comparison of the elevations of the distinctive reflectors (Table 1) indicates three faulting events.

The first faulting event occurred after deposition of reflector f and before deposition of reflector e, after glacial retreat. This faulting event is characterized by ~50 cm and ~45 cm of down-to-the-east offset on the western and eastern faults, respectively. The net down-to-the east offset across the zone was ~95 cm.

The second faulting event occurred after deposition of reflector c but before deposition of reflector b. Given the thickness of the section above reflector c as well as the estimated sedimentation rates (see section on Laminated Deep-Basin Deposits), this faulting event has an age of 12.5 to 7.5 ka. The movements resulted in ~90 cm of east-side-down offset on the western fault and ~75 cm of west-side-down offset (opposite to event 1) on the east-

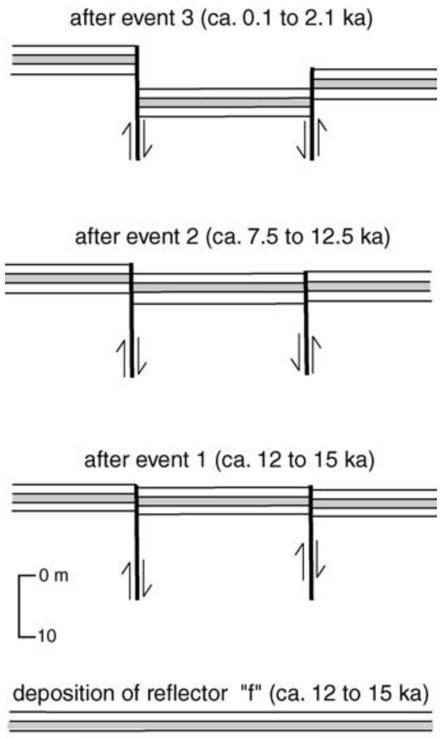

Figure 23. Schematic diagram showing inferred postglacial history of reflector f (shaded layer) in Lake Hotel fault zone (Table 1). Age estimates are based on inferred Holocene basinal sedimentation rate (60–100 cm/1000 yr) and on assumption that reflectors f and g are of latest glacial to early postglacial age. Note that the sense of slip on the eastern fault changes between the first and second events.

ern fault. The net down-to-the east slip across the zone was thus ~15 cm.

The third faulting event occurred after deposition of reflector a, which occurs at a depth of ~130 cm beneath the lake floor. This event resulted in ~580 cm of down-to-the east offset on the western fault and ~280 cm of down-to-the-west offset on the eastern fault. The cumulative down-to-the east slip across the zone during this event was thus ~300 cm. On the basis of estimated sedimentation rates (see section on Laminated Deep-Basin Deposits), this event has a maximum age of ca. 2.1 ka. There is no historic record of a large earthquake beneath northern Yellowstone Lake. Hence, this event must have occurred before about A.D. 1900.

Cumulative net down-to-the-east fault slip across this zone on the three events is ~4.1 m, yielding a postglacial slip rate of ~0.25–0.30 mm/yr and an earthquake recurrence interval of ~5000 yr. The net slip across the zone (95, 15, and 300 cm) in each faulting event varies substantially.

Other Faults

Truncated and/or offset seismic reflections occur on several other profiles. On line 98b (Fig. 4), for example, one or two faults upwarp and truncate basinal reflections; offset along the eastern fault is ~180 cm. The upwarping is unexpected in this extensional environment and is probably caused by the expulsion of hydrothermal gas or fluid through the vent that coincides with the fault. This fault and other similar structures do not form lineaments on the multibeam bathymetric map, and they typically cannot be traced for more than a few hundred meters with seismic reflection data despite the tight line spacing of our survey (Fig. 2). It is possible that many of these faults are the surface manifestations of deeper structures within the ring-fracture zone of the Yellowstone caldera (Christiansen, 2001).

DISCUSSION

Seismic reflection data reveal abundant evidence of latest Pleistocene and Holocene hydrothermal and tectonic activity in northern Yellowstone Lake. The identification of submerged shorelines adds to the record of lake-level change, which has served as the basis for understanding the Holocene behavior of the Yellowstone magmatic/geothermal system. Hydrothermal features and deposits are imaged in unprecedented detail, providing information on processes and hazards as well as important analogues for evaluation of similar features elsewhere. Documentation of the Lake Hotel fault aids earthquake-hazard assessment and demonstrates the utility of high-resolution seismic reflection data in paleoseismologic investigations.

Significance of Submerged Shoreline Terraces

The presence and chronology of the four submerged shoreline terraces adds an important element to understanding the postglacial history of Yellowstone Lake and the behavior of the Yellowstone magmatic/geothermal system. Pierce et al. (1993, 1997, 2002) and Locke and Meyer (1994) summarized constraints on the ages of elevated shoreline terraces, indicating a general decline in lake level from ca. 17 to 4 ka (emergent shoreline terraces S^{11} to S^{2}), down to ~3 m above the present shoreline. Pierce et al. (2002) stated that all lower shorelines (including those below lake level) are younger than 8 ka, consistent with lower amounts of deformation of submerged terraces (Fig. 15) compared to exposed emergent terraces (Meyer and Locke, 1986; Pierce et al., 2002). Pierce et al. (1997, 2002) dated the S^{-2} submerged terrace, ~3.4 m below the lake datum, at ca. 3 ka on the basis of ^{14}C dates on (1) wood associated with beach sands and gravels in Bridge Bay (Fig. 15), (2) charcoal in river gravel downstream from Fishing Bridge (Fig. 3), and (3) wood in a drowned valley at West Thumb (Fig. 1). The S^{-4} and S^{-3} submerged terraces are less prominent than the S^{-2} terrace and thus probably formed between 8 and 3 ka. The S^{-3} shoreline is poorly preserved and thus probably predates S^{-4}; we infer that S^{-3} was partly eroded and degraded first when it was emergent as lake level dropped to S^{-4} and then again when lake level rose through the S^{-3} elevation, climbing to S^{-2}. The S^{-1} terrace is probably younger than S^{-2}, an intermediate step on the rise to present lake level (S^{1}). The total drop in lake level from S^{2} to S^{-4} is ~15 m, and the subsequent rise from S^{-4} to S^{1} is ~12 m.

Locke and Meyer (1994) and Pierce et al. (1997, 2002) attributed the fluctuating lake levels recorded by the on-land and submerged shoreline terraces to uplift and subsidence of the lake outlet at Le Hardy Rapids (Fig. 1). The changes in lake-outlet elevation are controlled by magma intrusion or cooling and/or geothermal inflation and deflation. Smaller changes on a shorter time scale in the Yellowstone caldera (termed ''breathing'') have been well documented by geodetic and remote-sensing studies (Pelton and Smith, 1982; Dzurisin and Yamashita, 1987; Dzurisin et al., 1990, 1994; Wicks et al., 1998). The postglacial lake-level curve shown in Figure 15 therefore indicates long-term subsidence from ca. 15 to 5 Ma, followed by uplift from ca. 5 Ma to the present. Pierce et al. (1997) referred to this longer-term behavior as ''heavy breathing.''

Downfaulting of the lake outlet has also been suggested as a cause of lake-level fluctuation (Pierce et al., 1993; Tiller, 1995). Given the terrace chronology (Fig. 15), however, it is unlikely that movement along the Lake Hotel fault or associated structures near the lake outlet had a role in lowering the elevation of the lake outlet. Our data indicate that the largest of three ground-rupturing events on this zone occurred sometime in the past ~2100 yr, a time that apparently corresponds to a period of slow lake-level rise with no evidence of abrupt drops.

Climate change is not considered a viable hypothesis for lower lake levels and the occurrence of Holocene submerged terraces in Yellowstone Lake (Locke and Meyer, 1994; Pierce et al., 2002). For this hypothesis, an enormous decrease in precipitation relative to evaporation would be required in order to force closed-basin conditions. There is no independent evidence for such a climate change in the Yellowstone area (e.g., Baker, 1976; Waddington and Wright, 1974; Whitlock and Bartlein, 1993).

Geothermal Hazards

Mary Bay crater (Figs. 13, 16) and Elliott's crater (Fig. 14) are the world's largest known hydrothermal explosion craters (Browne and Lawless, 2001); thus, understanding their histories and the possibility of future large explosions in Yellowstone Lake is essential for hazard assessment. Effects of a large hydrothermal explosion in Yellowstone Lake could include fallout of explosion breccia, triggering of landslides on the lake margins, and seiche activity.

The Mary Bay crater is currently a significant center of geothermal activity, indicated by extremely high heat flow (Morgan et al., 1977), abundant vents (Figs. 13, 16), and the chaotic reflections that typify (attributed to hydrothermal gases and alteration) the crater-floor deposits. Given these circumstances, it is likely that there have been numerous hydrothermal explosions centered in Mary Bay since it formed at ca. 13 ka; however, none had sufficient energy to send ejecta onshore. A detailed coring investigation in and around Mary Bay is needed to evaluate the occurrence and frequency of post–13 ka explosions. At present, the large number of vents in the floor of the Mary Bay crater indicates that there is no efficient crater-wide seal or cap rock. Hence, the development of reservoir pressures greatly in excess of lithostatic and hydrostatic pressures beneath large parts of the Mary Bay crater seems unlikely, as does the possibility of imminent large-scale hydrothermal explosions.

Elliott's crater formed between ca. 13 and 8 ka and, in contrast to Mary Bay crater, has not continued to be a geothermal center. Sediments deposited on the crater floor are represented by high-frequency continuous reflections (Fig. 14), indicating that they are not significantly gas charged or hydrothermally altered. The crater floor is also flat, suggesting it is not currently inflated. The possibility of another large hydrothermal explosion from Elliott's crater in the near future thus seems unlikely.

Locations of present doming (Figs. 18, 20, 21) beneath the lake are here considered the most probable sites of future, large, hydrothermal explosions. Domes, responsible for considerable irregular relief on the lake floor, are most common in shallower parts of the lake near and along fissures and are least common in the deeper central lake basin and northwest subbasin (Fig. 3). This relationship suggests that shallower areas of the lake are relatively inflated by hydrothermal pressures compared to deeper parts of the lake. Some domes have been breached by vents (e.g., Figs. 18, 21), which presumably results in a decrease in reservoir confining pressures, arrested dome growth, and less chance of a large explosion. Thus, we think that future hydrothermal explosions will most likely occur in unbreached domed areas (e.g., Fig. 20).

The inferred terrace chronology suggests a lack of correlation between the lowest lake levels and large hydrothermal explosions. Muffler et al. (1971) suggested that such explosions can be triggered by abrupt decreases in hydrostatic confining pressures. Mary Bay and Elliott's craters formed between ca. 13 and 8 ka as the lake level decreased, and it is possible that their explosions coincided with rapid drops during that period. However, no large explosion in the lake correlates with the submerged shoreline terraces, when confining hydrostatic pressures would have been their lowest. Assuming that high lake levels correlate with crustal inflation and low lake levels correlate with deflation and lowering of the lake outlet, it may be that the thermal energy needed for development of hydrothermal explosion craters occurs primarily while the crust is relatively inflated. During these inflationary episodes, abrupt drops in confining pressures (forced by tectonics or climate?) could provide triggers for hydrothermal explosions.

Hazard Assessment of the Lake Hotel Fault

The Lake Hotel fault, with an apparent maximum event displacement of 300 cm, should be more than 20 km long on the basis of the regression analysis of Wells and Coppersmith (1994, their Fig. 12). By using our seismic reflection and bathymetric data (Figs. 2, 3), we can trace this fault for no more than 3 km. Deformation may, however, extend for considerable distance to the north and south as a distributed extensional zone.

Our data show that relief on both faults in the Lake Hotel zone terminates to the north. The S^{-2} submerged shoreline terrace, which predates the youngest (and largest) faulting event, is not offset by the Lake Hotel fault south of Lake Village (Figs. 3, 15). Furthermore, the Lake Hotel fault zone has not been detected along its trend north of the lake (Christiansen and Blank, 1975; Richmond, 1977a, 1977b). However, Pierce et al. (2002) mapped a north-northeast–trending normal fault on land ~250 m east of the Yellowstone Lake outlet and 450 m east of the trend of the eastern fault in the offshore Lake Hotel zone (Fig. 15). This fault offsets ca. 8 ka subaerial shoreline S^2 ~50 cm and ca. 10.5 ka shoreline S^4 ~100 cm and could represent a right-stepping en echelon section of the Lake Hotel fault zone.

To the south of line Y74 (Fig. 3), the bathymetric data suggest that the Lake Hotel fault zone may intersect line Y40 (Fig. 20) through a zone of chaotic reflections on the western margin of a small basin, probably as a single splay. Line Y98a (Fig. 7), our first east-west tie line south of Stevenson Island, shows an unfaulted 15-m-thick section of basinal strata on the trend of the Lake Hotel fault, ruling out linear projection of this fault zone this far to the south. We therefore argue that the northwest- to north-northeast–trending fissure zones east and west of Stevenson Island (Fig. 2) and several small faults (e.g., line Y98b; Fig. 3) accommodate and distribute the extension manifested in the Lake Hotel fault zone to the north.

Other faults mapped south of our study area are probably also related to the Lake Hotel fault. About 15 km south of and on the same trend as the Lake Hotel fault, Richmond (1974) mapped an ~5-km-long north-trending normal fault at the east end of the Flat Mountain Arm (Fig. 1) that Locke et al. (1992) subsequently named the Eagle Bay fault. Locke et al. suggested just one postglacial faulting event, occurring in the past 4500 yr and yielding scarps as high as 8.9 m. Between the Lake Hotel and Eagle Bay fault zones, Tiller (1995) interpreted a postglacial normal fault with as much as 17 m of offset on a northwest-trending seismic reflection profile between Dot and Frank Islands (Fig. 1).

Available data therefore indicate that a zone of north-trending normal faults and/or fissures extends both north and south of the Lake Hotel fault zone over a cumulative length of at least 25 km. It is possible that this zone is a single distributed extensional fault zone characterized by several discontinuous segments that connect at depth. If this is the case, then rupture propagates to the surface in a highly heterogeneous manner. Recent seismicity indicates that the thickness of seismogenic crust in the Yellowstone caldera is only ~5 km

(Smith and Braile, 1984) because of high heat flow. Given this thickness and the suggested maximum length (25 km) of the fault zone, the rupture area for a potential earthquake could be as large as 125 km^2. A rupture area of this size could generate an earthquake as large as 6.5, on the basis of regressions comparing fault rupture and earthquake magnitude (Wells and Coppersmith, 1994; their Fig. 16). If the fault is shorter or if rupture is limited to short segments, the potential rupture area and earthquake magnitude decrease substantially. For example, rupture of only the ~3-km-long Lake Hotel segment of this zone (rupture area of ~15 km^2) would yield an earthquake of magnitude 5.3.

The latest and largest rupture on the Lake Hotel fault zone does not correlate with lower lake level or with large, sublacustrine hydrothermal explosions. It is possible that movement on the Lake Hotel fault zone could locally alter subsurface ''plumbing'' in the Yellowstone caldera and, in that way, help trigger a hydrothermal explosion, but that hypothesis cannot be rigorously tested with available data. The first two faulting events on the Lake Hotel zone (Table 1; Fig. 23) occurred prior to ca. 7.5 ka and could correlate with the Mary Bay or Elliott's hydrothermal explosions.

Landsliding on the lake margins might be triggered by strong ground motions and thus could correlate with Lake Hotel zone faulting and/or with Mary Bay and Elliott's explosions. However, equally strong ground motions around Yellowstone Lake might be generated by rupture of other nearby faults (e.g., the Hebgen fault, Myers and Hamilton, 1964) or by hydrothermal explosions from other nearby geothermal areas.

CONCLUSIONS

Our work in northern Yellowstone Lake reinforces the importance of detailed geophysical investigations of lakes in active volcanic settings (e.g., Newhall et al., 1987; Bacon et al., 2002). The seismic reflection survey of northern Yellowstone Lake images active geothermal features and faults with unprecedented resolution, providing essential information for understanding geologic processes, assessment of geologic hazards, and recognition of comparable features in other subaqueous volcanic environments.

Seismic reflection data from northern Yellowstone Lake document the distribution, size, geometry, and relative age of geothermal features, including the world's largest known hydrothermal explosion craters, asymmetric crater ejecta, and vents and domes of variable size and concentration. Mary Bay crater (ca. 13 ka) continues to be a center of geothermal activity, possibly including small hydrothermal explosions, whereas Elliott's crater (ca. 13–8 ka) has been relatively quiescent for several thousand years. Domed areas that are unbreached by vents are considered the most likely sites of future large hydrothermal explosions. Submerged shoreline terraces complete the postglacial record of ''heavy breathing'' of the Yellowstone caldera, an essential context for understanding past and future caldera behavior as well as recent, smaller-scale, caldera uplift and subsidence. A distributed extensional zone within northern Yellowstone Lake is characterized by both normal faults and by linear fissures. Documentation of the Lake Hotel fault zone provides estimates of offset and recurrence interval and demonstrates the utility of high-resolution seismic reflection data in paleoseismology.

ACKNOWLEDGMENTS

This research was supported by the Mineral Resource Surveys Program, Climate History Program, Venture Capital Fund, and Northern Rocky Mountain Research Center of the U.S. Geological Survey; the National Park Service; and the Yellowstone Foundation. We thank Eric L. White, Dave Lovalvo, Steve Harlan, and Jim Waples for help with data acquisition. Stimulating discussions with Mike Machette and Brian Sherrod helped shape and clarify some of our interpretations. Brian Sherrod, Bob Christiansen, Daniel Belknap, William Locke, and Henry Mullins provided constructive reviews, and Sherrod provided a preliminary version of Figure 1.

REFERENCES CITED

Bacon, C.R., 1983, Eruptive history of Mount Mazama and Crater Lake caldera, Cascade Range, U.S.A.: Journal of Volcanology and Geothermal Research, v. 18, p. 57–115.

Bacon, C.R., Gardner, J.V., Mayer, L.A., Buktenica, M.W., Dartnell, P., Ramsey, D.W., and Robinson, J.E., 2002, Morphology, volcanism, and mass wasting in Crater Lake, Oregon: Geological Society of America Bulletin, v. 114, p. 675–692.

Baker, R.G., 1976, Late Quaternary vegetation history of the Yellowstone Lake basin, Wyoming: U.S. Geological Survey Professional Paper 729E, p. E1–E48.

Benson, N.G., 1961, Limnology of Yellowstone Lake in relation to the Cutthroat trout: U.S. Fish and Wildlife Service, Bureau of Sport Fisheries and Wildlife Research Report 56, 33 p.

Bradley, W.C., and Griggs, G.B., 1976, Form, genesis, and deformation of central California wave-cut terraces: Geological Society of America Bulletin, v. 87, p. 553–570.

Browne, P.R.L., and Lawless, J.V., 2001, Characteristics of hydrothermal eruptions, with examples from New Zealand and elsewhere: Earth-Science Reviews, v. 52, p. 299–331.

Christiansen, R.L., 1984, Yellowstone magmatic evolution: Its bearing on understanding large volume explosive volcanism, *in* Explosive volcanism: Washington, D.C., National Academy of Sciences, p. 84–95.

Christiansen, R.L., 2001, The Quaternary and Pliocene Yellowstone Plateau volcanic province: U.S. Geological Survey Professional Paper 729-G, 120 p.

Christiansen, R.L., and Blank, H.R., 1975, Geologic map of the Canyon Village quadrangle, Yellowstone National Park, Wyoming: U.S. Geological Survey Map GQ-1192, scale 1:62,500.

Dzurisin, D., and Yamashita, K.M., 1987, Vertical surface displacement at Yellowstone caldera, 1976–1987: Journal of Geophysical Research, v. 92, p. 13,767–13,777.

Dzurisin, D., Savage, J.C., and Fournier, R.O., 1990, Recent crustal subsidence of Yellowstone caldera, Wyoming: Bulletin of Volcanology, v. 52, p. 247–270.

Dzurisin, D., Yamashita, K.M., and Kleinman, J.W., 1994, Mechanisms of crustal uplift and subsidence at the Yellowstone caldera, Wyoming: Bulletin of Volcanology, v. 56, p. 261–270.

Fader, G.B.J., 1997, The effects of shallow gas on seismic reflection profiles, *in* Davies, T.A., Bell, Trevor, Cooper, A.K., Josenhans, H., Polyak, L., Solheim, A., Stoker, M.S., and Stravers, J.A., eds., Glaciated continental margins: An atlas of acoustic images: London, Chapman and Hall, p. 29–30.

Finn, C.A., and Morgan, L.A., 2002, High-resolution aeromagnetic mapping of volcanic terrain in Yellowstone National Park: Journal of Volcanology and Geothermal Research, v. 115, p. 207–231.

Foit, F.F., Mehringer, P.J., Jr., and Sheppard, J.C., 1993, Age, distribution, and stratigraphy of Glacier Peak tephra in eastern Washington and western Montana, United States: Canadian Journal of Earth Sciences, v. 30, p. 535–552.

Hallett, D.J., Hills, L.V., and Clague, J.J., 1997, New accelerator mass spectrometry radiocarbon ages for the Mazama tephra layer from Kootenay National Park, British Columbia, Canada: Canadian Journal of Earth Sciences, v. 34, p. 1202–1209.

Hamilton, W.L., 1987, Water level records used to evaluate deformation within the Yellowstone caldera, Yellowstone National Park: Journal of Volcanology and Geothermal Research, v. 31, p. 205–215.

Hamilton, W.L., and Bailey, A.L., 1988, Holocene deformation deduced from shorelines at Yellowstone Lake, Yellowstone caldera: Historical summary and implications [abs.]: Eos (Transactions, American Geophysical Union), v. 69, p. 1472.

Hamilton, W.L., and Bailey, A.L., 1990, Holocene deformation history of the Yellowstone caldera at Yellowstone Lake inferred from abandoned shorelines and sediments: Yellowstone Physical Science Laboratory Division of Research, Report 90–3, 24 p.

Kaplinski, M.A., 1991, Geomorphology and geology of Yellowstone Lake, Yellowstone National Park, Wyoming [M.S. thesis]: Flagstaff, Northern Arizona University, 80 p.

Licciardi, J.M., Clark, P.U., Brook, E.J., Pierce, K.L., Murz, M.D., Elmore, David, and Sharka, Pankaj, 2001, Cosmogenic ^{3}He and ^{10}Be chronologies of the late Pinedale northern Yellowstone ice cap, Montana, USA: Geology, v. 29, p. 1095–1098.

Locke, W.W., and Meyer, G.A., 1994, A 12,000 year record of vertical deformation across the Yellowstone caldera margin: The shorelines of Yellowstone Lake: Journal of Geophysical Research, v. 99, p. 20,079–20,094.

Locke, W.W., Meyer, G.A., and Pings, J.C., 1992, Morphology of a postglacial fault scarp across the Yellowstone (Wyoming) caldera margin and its implications: Seismological Society of America Bulletin, v. 82, p. 511–516.

Meyer, G.A., and Locke, W.W., 1986, Origin and deformation of Holocene shoreline terraces, Yellowstone Lake, Wyoming: Geology, v. 14, p. 699–702.

Mitchum, R.M., Jr., Vail, P.R., and Sangree, J.B., 1977, Seismic stratigraphy and global changes of sea level: Part 6. Stratigraphic interpretation of seismic reflection patterns in depositional sequences, *in* Payton, C.E., ed., Seismic stratigraphy: Applications to hydrocarbon exploration: American Association of Petroleum Geologists Memoir 26, p. 117–134.

Morgan, P., Blackwell, D.D., and Spafford, R.E., 1977, Heat flow measurements in Yellowstone Lake and the thermal structure of the Yellowstone caldera: Journal of Geophysical Research, v. 82, p. 3719–3732.

Morgan, L.A., Shanks, W.C., Lovalvo, D.A., Johnson, S.Y., Stephenson, W.J., Pierce, K.L., Harlan, S.S., Lee, G., Webring, M., Finn, C.A., Sweeney, R., and Balistrieri, L., 2003, Volcanic and hydrothermal processes above a cooling magma chamber: Results from high-resolution sonar imaging, seismic reflection, and submersible surveys of Yellowstone Lake: Journal of Volcanology and Geothermal Research (in press).

Muffler, L.J.P., White, D.E., and Truesdell, A.H., 1971, Hydrothermal explosion craters in Yellowstone National Park: Geological Society of America Bulletin, v. 82, p. 723–740.

Myers, W.B., and Hamilton, W., 1964, Deformation accompanying the Hegben Lake earthquake of August 17, 1959: U.S. Geological Survey Professional Paper 435-I, p. 55–98.

Newhall, C.G., Paull, C.K., Bradbury, J.P., Higuera-Gundy, A., Poppe, L.J., Self, S., Bonar Sharpless, N., and Ziagos, J., 1987, Recent geologic history of Lake Atitlan, a caldera lake in western Guatemala: Journal of Volcanology and Geothermal Research, v. 33, p. 81–107.

Otis, R.M., Smith, R.B., and Wold, R.J., 1977, Geophysical surveys of Yellowstone Lake, Wyoming: Journal of Geophysical Research, v. 82, p. 3705–3717.

Pelton, J.R., and Smith, R.B., 1982, Contemporary vertical surface displacements in Yellowstone National Park: Journal of Geophysical Research, v. 87, p. 2745–2761.

Pierce, K.L., 1979, History and dynamics of glaciation in the northern Yellowstone National Park area: U.S. Geological Survey Professional Paper 729-F, 90 p.

Pierce, K.L., Cannon, K.P., Crothers, G.M., Meyer, G.A., and Rubin, Meyer, 1993, Backflooding upstream from the resurgent dome of the 0.6 Ma Yellowstone caldera: Two backflooding cycles in the last 8,000 years [abs.]: Eos (Transactions, American Geophysical Union), v. 74, p. 592.

Pierce, K.L., Cannon, K.P., and Meyer, G., 1997, Yellowstone caldera ''heavy breathing'' based on Yellowstone Lake and River changes in post-glacial time: Eos (Transactions, American Geophysical Union), v. 78, p. F802.

Pierce, K.L., Cannon, K.P., Meyer, G.A., Trebesch, M.J., and Watts, R.D., 2002, Post-glacial inflation-deflation cycles, tilting, and faulting in the Yellowstone caldera based on Yellowstone Lake shorelines: U.S. Geological Survey Open-File Report 02–142, 30 p.

Remsen, C.C., Klump, J.V., Kaster, J.L., Paddock, R., Anderson, P., and Maki, J.S., 1990, Hydrothermal springs and gas fumaroles in Yellowstone Lake, Yellowstone National Park, Wyoming: National Geographic Research, v. 6, p. 509–516.

Richmond, G.M., 1974, Surficial geologic map of the Frank Island quadrangle, Yellowstone National Park, Wyoming: U.S. Geological Survey Miscellaneous Geologic Investigations Map I-642, scale 1:62,500.

Richmond, G.M., 1977a, Surficial geologic map of the Canyon Village quadrangle, Yellowstone National Park, Wyoming: U.S. Geological Survey Miscellaneous Geologic Investigations Map I-652, scale 1:62,500.

Richmond, G.M., 1977b, Surficial geologic history of the Canyon Village quadrangle, Yellowstone National Park, Wyoming, for use with Map I-652: U.S. Geological Survey Bulletin 1427, 35 p.

Shero, B.R., 1977, An interpretation of temporal and spatial variations in the abundance of diatom taxa in sediments from Yellowstone Lake, Wyoming [Ph.D. thesis]: Laramie, University of Wyoming, 178 p.

Shuey, R.T., Ugland, R.O., and Schmit, C.R., 1977, Magnetic properties and secular variation in cores from Yellowstone and Jackson Lakes, Wyoming: Journal of Geophysical Research, v. 82, p. 3739–3746.

Smith, R.B., and Arabasz, W.J., 1991, Seismicity of the Intermountain seismic belt, *in* Slemmons, D.B., Engdahl, E.R., Zoback, M.D., and Blackwell, D.D., eds., Neotectonics of North America: Geological Society of America, North America Decade Map, v. 1, p. 185–228.

Smith, R.B., and Braile, L.W., 1984, Crustal structure and evolution of an explosive silicic volcanic system at Yellowstone National Park, *in* Explosive volcanism, inception, evolution, and hazards: Washington, D.C., National Academy Press, p. 96–109.

Smith, R.B., Shuey, R.T., Pelton, J.R., and Bailey, J.P., 1977, Yellowstone hot spot: Contemporary tectonics and crustal properties from earthquake and aeromagnetic data: Journal of Geophysical Research, p. 3665–3676.

Tiller, C.C., 1995, Postglacial sediment stratigraphy of large lakes in greater Yellowstone—Scenarios of tectonic and climatic forcing [M.S. thesis]: Minneapolis, University of Minnesota, 193 p.

U.S. Geological Survey, 1972, Geologic map of Yellowstone National Park: U.S. Geological Survey Miscellaneous Investigations Map I-711, scale 1:250,000.

Waddington, J.C.B., and Wright, H.E., Jr., 1974, Late Quaternary vegetation changes on the east side of Yellowstone Park, Wyoming: Quaternary Research, v. 4, p. 175–184.

Wells, D.L., and Coppersmith, K.J., 1994, New empirical relationships among magnitude, rupture length, rupture width, rupture area, and surface displacement: Seismological Society of America Bulletin, v. 84, p. 974–1002.

Whitlock, C., and Bartlein, P.J., 1993, Spatial variations of Holocene climatic change in the Yellowstone region: Quaternary Research, v. 39, p. 231–238.

Wicks, C., Jr., Thatcher, W., and Dzurisin, D., 1998, Migration of fluids beneath Yellowstone caldera inferred from satellite radar interferometry: Science, v. 282, p. 458–462.

Wold, R.J., Mayhew, M.A., and Smith, R.B., 1977, Bathymetric and geophysical evidence for a hydrothermal explosion crater in Mary Bay, Yellowstone Lake, Wyoming: Journal of Geophysical Research, v. 82, p. 3733–3738.

Zdanowicz, C.M., Zielinski, G.A., and Germani, M.S., 1999, Mount Mazama eruption—Calendrical age verified and atmospheric impact assessed: Geology, v. 27, p. 621–624.

Manuscript Received by the Society 15 January 2002
Revised Manuscript Received 6 November 2002
Manuscript Accepted 19 February 2003

Printed in the USA